Chair of High-Power Converter Systems
TUM School of Engineering and Design
Technical University of Munich
Prof. Dr.sc. ETH Zürich Marcelo Lobo Heldwein

Research and Development of Power Control Middleware Algorithms (PLL, MPPT)

Haoheng Li

Research and Development of Power Control Midware Algorithms (PLL, MPPT)

Report of Research Internship

to pass the research internship

Master of Science
(M.Sc.)

in Power Engineering

at Technical University of Munich

Submitted by Haoheng Li
Matriculation Number: 03797669
haoheng.li@tum.de

on Thursday 16th October, 2025

Supervisor: Maia de Sousa, Dr. Gean
Chair of High-Power Converter Systems
Technical University of Munich
gean.sousa@tum.de

Declaration

The work in this repoort is based on research carried out at the Chair of High-Power Converter Systems, Technical University of Munich (TUM) supervised by Maia de Sousa, Dr. Gean. No part of this report has been submitted elsewhere for any other academic degree or qualification and it is all my own work unless referenced to the contrary in the text.

Place, Date, Signature

Abstract

This report presents the research and development of power control middleware algorithms, specifically focusing on Phase-Locked Loop (PLL) and Maximum Power Point Tracking (MPPT) techniques. The research internship was conducted at Infineon Technologies AG, under the supervision of Dr. Gean Maia de Sousa at the Chair of High-Power Converter Systems, TUM. The objective of this research is to design and evaluate the performance of PLL and MPPT algorithms in power electronic systems, which will finally outcome a repository containing the developed algorithms using Model Based Design (MBD) approach. The outcome can be seen in the GitHub repository: `https://github.com/labourer-Lucas/Research-Inernship-PLL-and-MPPT`.

Contents

CHAPTER 1

Introduction

1.1 Background of the Internship

I have been a research intern at Infineon Technologies AG since July, 2025, working as a Power Control Algorithm Intern. I was responsible for developing and implementing middleware control algorithms for power electronics systems, specifically focusing on PLL and MPPT algorithms using Model Based Design (MBD). With aid of MATLAB/Simulink, I designed the algorithms and tested them in a simulated environment. Finally, I generated C code from the Simulink models using Embedded Coder.

1.1.1 Company Overview

Infineon Technologies AG is a global leader in semiconductor solutions, providing innovative technologies for various applications, including automotive, industrial, and consumer electronics.

I was working in the Power & Sensor Systems (PSS) division, which focuses on developing advanced sensor solutions and power management technologies. The PSS division powers Infineon's decarbonization and digitalization vision with a wide range of energy-efficient and digital solutions.

1.1.2 Project Overview

The project "Power Control Middleware" aims to develop and middleware control algorithms for power electronics systems, such as PLL, MPPT, Kalman Filter, and 3-zero-3-pole filters. During my internship, I focused on the PLL and MPPT algorithms.

1.2 Objective of the Internship

The main objectives of my internship were to:

- Develop and implement PLL and MPPT algorithms using MBD
- Test the algorithms in a simulated environment using MATLAB/Simulink and evaluate their performance
- Generate C code from the Simulink models using Embedded Coder
- Document the development process and results in a comprehensive report

1.2.1 Phase-Locked Loop (PLL)

Grid synchronization is the process by which power converters, especially those connected to renewable energy sources, ensure that the power injected by the inverter is aligned with the grid. This includes estimating and matching the phase angle, frequency, and voltage magnitude.

Grid synchronization can be achieved using various control techniques. The primary tool for achieving this is PLL. The latter consists of a feedback control loop that follows the frequency and phase of its input signal. In grid-tied applications, the PLL input is the grid voltage. Moreover, some advanced grid synchronization methods combine the PLL with filters applied to the input voltage. Such a combination allows for robust and precise estimation of the above-mentioned grid parameters even under unbalanced voltages, harmonic distortions, or voltage sags.

In my internship, I developed and implemented synchronous reference frame PLL (SRF-PLL), Double Decoupled Synchronous Reference Frame (DDSRF) PLL, Second-Order Generalized Integrators (SOGI) PLL, Dual-Second-Order Generalized Integrators (DSOGI) PLL, and Multiple Second-Order Generalized Integrators (MSOGI) PLL.

1.2.2 Maximum Power Point Tracking (MPPT)

MPPT is a family of control algorithms that aims at optimizing the use of a power source that possesses a fluctuating power profile.

In my research internship, I focus on developing the MPPT algorithms for DC optimizers, which are power electronic devices that are connected to individual solar panels in a photovoltaic (PV) system. I developed and implemented Perturb and Observe (P&O) and Incremental Conductance (InC) MPPT algorithms.

1.3 Structure of the Report

The first chapter introduces the background and objectives of the internship. The second chapter provides a detailed overview of the PLL and MPPT algorithms, including their principles, types, and applications. The third chapter describes the deesign and implementation of the PLL and MPPT algorithms using MBD, including the Simulink models. The fourth chapter presents

the testing and evaluation of the algorithms in a simulated environment, including performance analysis and results. Finally, the fifth chapter concludes the report with a summary of the work done, challenges faced, and future work suggestions.

CHAPTER 2

Algorithm Development

2.1 Overview of PLL and its Applications and Development

The increasing penetration of renewable energy into the grid necessitates the employment of grid synchronization techniques to ensure proper integration and stability of the system. Several grid synchronization techniques are available, among which the PLL method has proven to be the more employed one owing to its simplicity and robustness.

Despite being able to provide effective operation of the system under variable grid conditions this technique faces certain technological challenges. This paper studies, in detail, the various PLL techniques that are implemented in the Renewable Energy Sectorsuch as Synchronous Reference Frame (SRF-PLL), Decoupled Double Synchronous Reference Frame (DDSRF-PLL), Second Order General Integrator (SOGI-PLL), Dual Second Order General Integrator (DSOGI-PLL), and Multi Second Order General Integrator (MSOGI-PLL). The different techniques of the PLL are compared and analyzed based on their efficiency, response to voltage and frequency deviations, complexity, and stability. SRF-PLL gives excellent response under balanced grid conditions, but E-PLL, FLL and SOGI based PLLs are more efficient to address unbalanced grid conditions. The limitations of the PLL technique such as reduced stability margin and manufacturing costs, has lead to the development of improved and new PLLs, which are under research.

2.2 Synchronous Reference Frame PLL

2.2.1 SRF-PLL concept

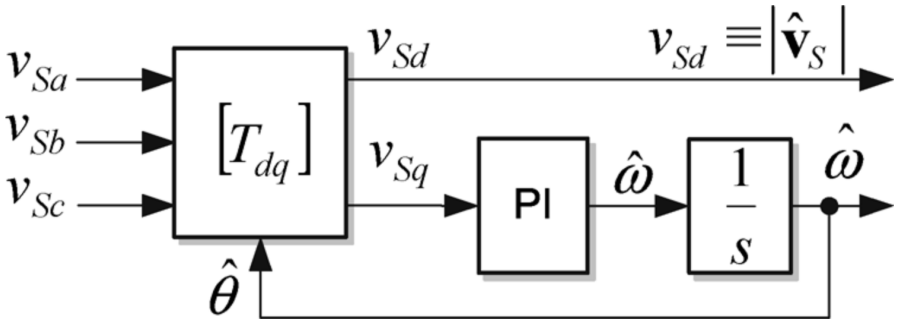

Figure 2.1: Block diagram of a typical SRF-PLL

A synchronous reference frame PLL is a basic type of phase-locked loop based on the Park transform [1]. In a nutshell, the SRF PLL is built using a Park transformation that acts as a phase detector, a low-pass filter (LPF) usually in the form of a PI regulator, and a voltage-controlled oscillator (VCO) typically made from an integrator. The objective of this PLL is then to minimize either the direct or quadrature axis reference voltage. This will then ensure that the phase angle of the rotating reference frame of the park transformation matches the phase angle of the utility grid voltage vector. The block diagram of a typical SRF-PLL is shown in

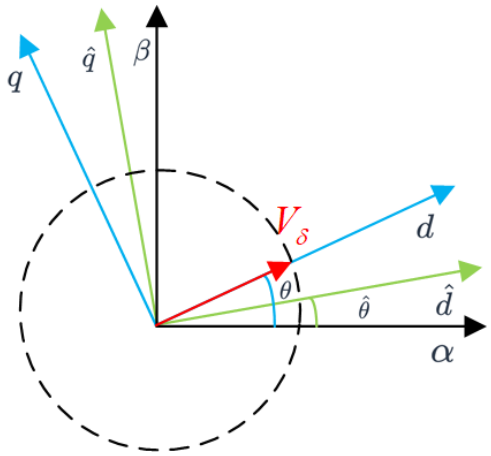

Figure 2.2: $d-q$ and $\hat{d}-\hat{q}$ Frame

Fig. 2.1. In the conventional SRF-PLL, the three-phase voltage vector is translated from the abc reference frame to the dq reference frame using the Park transformation. The angular position of this dq reference frame is controlled by a feedback loop which regulates the q component to

zero. Therefore in steady-state, the d component depicts the voltage vector amplitude and its phase is determined by the output of the feedback loop.

As shown in Figure 2.2 ,the actual phase angle of V_δ is θ, and the phase angle estimated by the PLL is $\hat{\theta}$. The corresponding $d-q$ and $\hat{d}-\hat{q}$ are rotating coordinate systems. Define $\delta = \theta - \hat{\theta}$, then

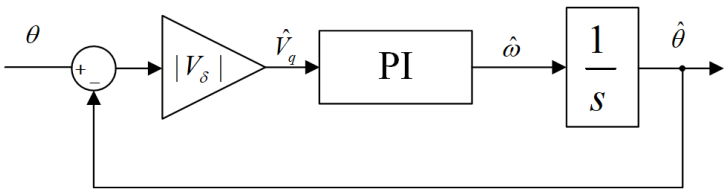

Figure 2.3: Block diagram of SRF-PLL in small signal model

$$\hat{V}_q = V_\delta \cdot \sin(\delta) \tag{2.1}$$

When δ is very small, $\sin(\delta) \approx \delta = \theta - \hat{\theta}$, and thus the control block diagram of the PLL can be depicted.

Figure 2.3 shows the small signal model of the SRF-PLL. However, in practical applications, this model is sensitive to the variation of the grid voltage amplitude. Thus, in order to compensate for that, we are going to design a normalized PLL in this section. The block diagram of normalized PLL is shown in Figure 2.4.

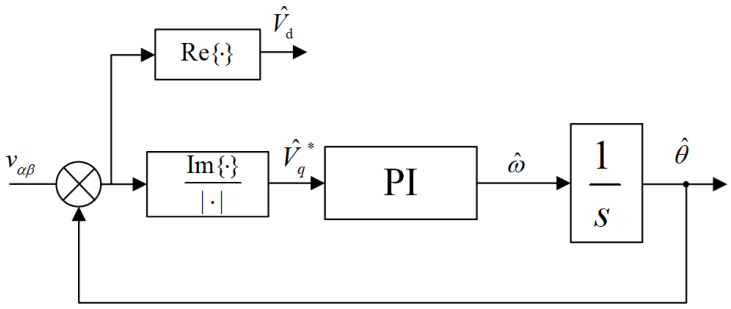

Figure 2.4: Block diagram of normalized SRF-PLL

Therefore, the close loop transfer function of the system can be written as:

$$G_{cl}(s) = \frac{\hat{\theta}(s)}{\theta(s)} = \frac{K_p s + K_i}{s^2 + K_p s + K_i} \tag{2.2}$$

where K_p and K_i are the proportional and integral gains of the PI controller, respectively. The natural frequency ω_n and damping ratio ζ of the system can be defined as:

$$\omega_n = \sqrt{K_i} \tag{2.3}$$

$$\zeta = \frac{K_p}{2\sqrt{K_i}} \tag{2.4}$$

In practical applications, the SRF-PLL is usually designed with a damping ratio of $\zeta = 0.707$ to ensure a good dynamic response without overshoot. The natural frequency ω_n is typically chosen to be arround 30Hz. A higher value of ω_n results in a faster dynamic response but may also lead to increased sensitivity to noise and harmonics in the grid voltage.

2.2.2 SRF-PLL under different grid conditions

To simply test the performance of the SRF-PLL under different grid conditions, a simulation is carried out in MATLAB/Simulink. The parameters of the SRF-PLL are chosen with a natural frequency of $\omega_n = 50Hz$ and a damping ratio of $\zeta = 0.707$.

The result of SRF-PLL under balanced grid conditions with a phase shift of $180°$ at $t = 0.1s$ is shown in Figure 2.5. It can be observed that the SRF-PLL can quickly track the phase angle of the grid voltage.

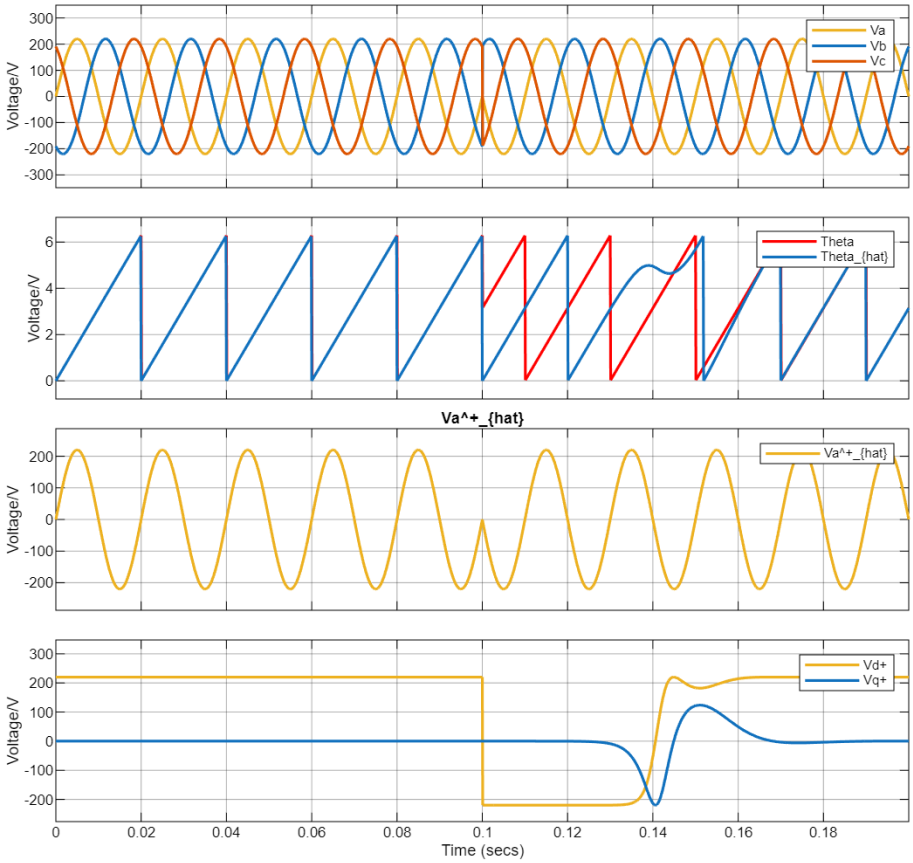

Figure 2.5: Response of the SRF-PLL with a phase shift at t=0.1s under balanced conditions. Utility voltage [V], Detected phase angle [rad], Fundamental voltage [V] and SRF axes voltage [V]

The result of SRF-PLL under unbalanced grid conditions with a negative sequence component of 30% and a phase shift of $180°$ at $t = 0.1s$ is shown in Figure 2.6. It can be observed that the SRF-PLL can still track the phase angle of the grid voltage, but with some oscillations

in the detected phase angle due to the unbalance in the grid voltage. In addition, the d and q axis voltages also show oscillations at twice the fundamental frequency, which can affect the performance of the PLL.

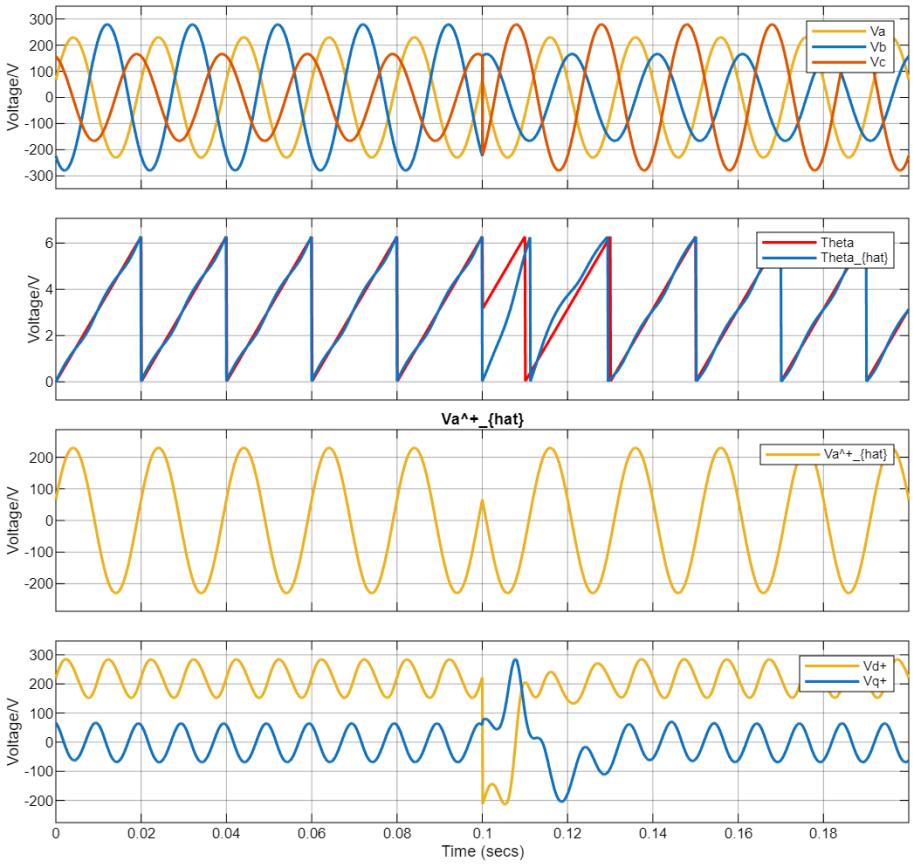

Figure 2.6: Response of the SRF-PLL with a phase shift at t=0.1s under unbalanced conditions. Utility voltage [V], Detected phase angle [rad], Fundamental voltage [V] and SRF axes voltage [V]

The result of SRF-PLL under grid conditions with 30% of the 5th harmonics and a phase shift of $180°$ at $t = 0.1s$ is shown in Figure 2.7. It can be observed that the SRF-PLL can still track the phase angle of the grid, but with some oscillations in the detected phase angle due to the presence of harmonics in the grid voltage. The d and q axis voltages also show oscillations at the harmonic frequencies, which can affect the performance of the PLL.

In conclusion, the SRF-PLL is a simple and effective method for grid synchronization under balanced grid conditions. However, its performance can be affected by unbalanced grid conditions and the presence of harmonics in the grid voltage. Therefore, for applications where the grid conditions are expected to be unbalanced or distorted, more advanced PLL techniques should be disgussed in the following sections.

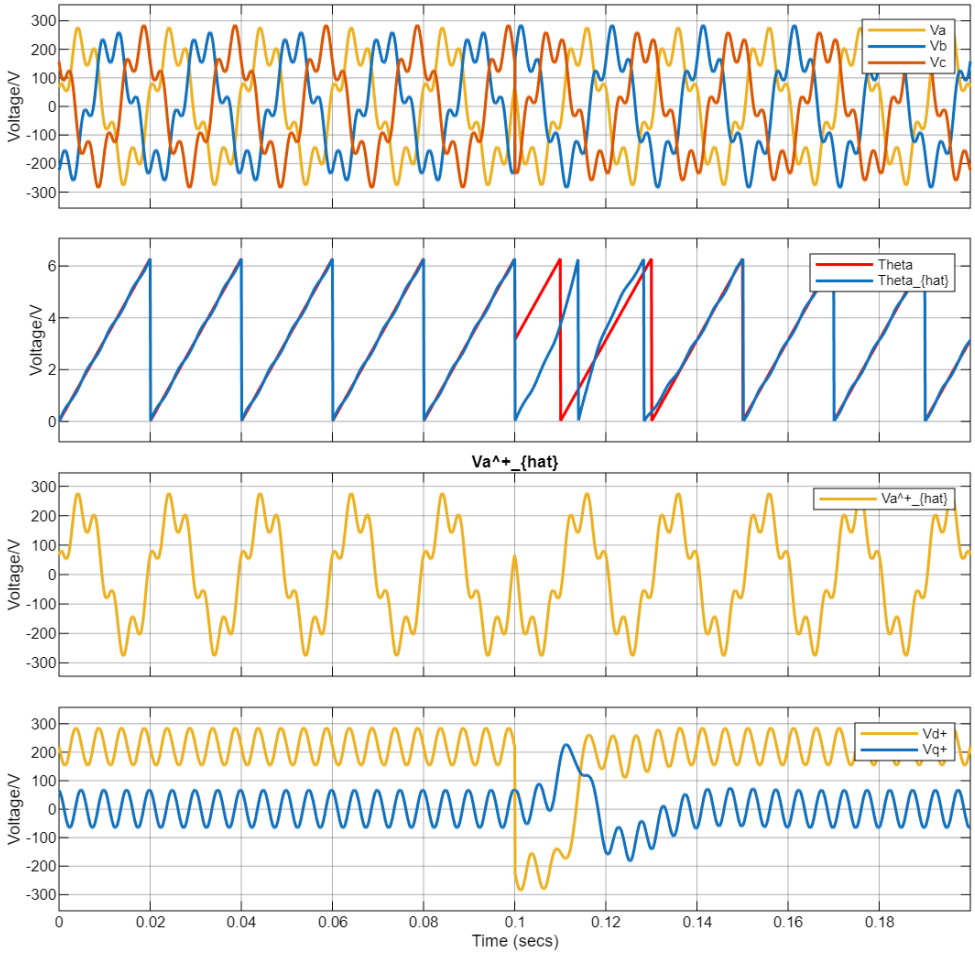

Figure 2.7: Response of the SRF-PLL with a phase shift at t=0.1s under grid conditions with 30% of the 5th harmonics. Utility voltage [V], Detected phase angle [rad], Fundamental voltage [V] and SRF axes voltage [V]

2.3 Decoupled Double Synchronous Reference Frame PLL

2.3.1 DDSRF-PLL concept

Thanks to its simplicity and performance under nominal conditions, the SRF-PLL has become the PLL of choice for applications where robustness against disturbances is not required. However, in the presence of unbalance in the grid voltage, an oscillating term at twice the fundamental frequency appears after the Park transform. The DDSRF-PLL effectively addresses this issue by using a decoupling network to separate the positive and negative sequence components, ensuring accurate detection even under unbalanced voltages [2].

The grid is subject to varying conditions which result in imbalances in the phase voltages. From the theory of symmetrical components we know that any unbalanced three phase system can be reduced to two symmetrical systems and zero component. The behavior of unbalanced voltages on park and clark transform is analyzed in section below.

Now an unbalanced three phase system can be written as summation of balanced three phase

systems; one rotating with the sequence of the three phase quantities called the positive sequence and one rotating in the opposite sequence called the negative sequence, whhich is shown in Figure 2.8.

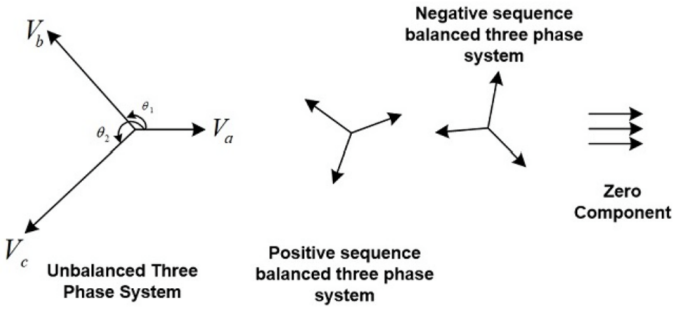

Figure 2.8: Unbalanced and balanced Three Phase Systems

The mathamatical representation of the unbalanced three phase system is given as:

$$v = V^{+1}\begin{bmatrix}\cos(wt)\\ \cos(wt-2\pi/3)\\ \cos(wt-4\pi/3)\end{bmatrix} + V^{-1}\begin{bmatrix}\cos(wt)\\ \cos(wt-4\pi/3)\\ \cos(wt-2\pi/3)\end{bmatrix} + V^{0}\begin{bmatrix}1\\1\\1\end{bmatrix} \tag{2.5}$$

If we apply the Clark transformation to the symmetrical components, we get the following results:

$$\nu_{\alpha\beta} = T_{abc->\alpha\beta}\cdot\nu = \frac{2}{3}\begin{bmatrix}1 & -\frac{1}{2} & -\frac{1}{2}\\ 0 & \frac{\sqrt{3}}{2} & -\frac{\sqrt{3}}{2}\\ \frac{1}{2} & \frac{1}{2} & \frac{1}{2}\end{bmatrix}\cdot\nu = V^{+1}\begin{bmatrix}\cos(wt)\\ \sin(wt)\end{bmatrix} + V^{-1}\begin{bmatrix}\cos(-wt)\\ \sin(-wt)\end{bmatrix} \tag{2.6}$$

Taking the projections on the rotating reference frame, we observe that any negative sequence component appears with twice the frequency on the positive sequence rotating frame axis and vice versa.

$$\begin{cases} \nu_{dq+} = T^{*}_{abc->dq0+}\nu_{\alpha\beta} = \begin{bmatrix}\cos(\omega t) & \sin(\omega t)\\ -\sin(\omega t) & \cos(\omega t)\end{bmatrix} = V^{+1}\begin{bmatrix}1\\0\end{bmatrix} + V^{-1}\begin{bmatrix}\cos(-2wt)\\ \sin(-2wt)\end{bmatrix} \\ \nu_{dq-} = T^{*}_{abc->dq0-}\nu_{\alpha\beta} = \begin{bmatrix}\cos(\omega t) & -\sin(\omega t)\\ \sin(\omega t) & \cos(\omega t)\end{bmatrix} = V^{+1}\begin{bmatrix}\cos(-2wt)\\ \sin(-2wt)\end{bmatrix} + V^{-1}\begin{bmatrix}1\\0\end{bmatrix} \end{cases} \tag{2.7}$$

This can cause errors in the control loop and estimation of the grid angle and needs to taken into account while designing a phase locked loop for three phase grid connected application, like shown in Figure .

Hence assuming the instance just before the PLL is locked to the positive vector, the grid voltages can be written as :

$$v = V^{+1}\begin{bmatrix}\cos(wt+\phi_1)\\ \cos(wt-2\pi/3+\phi_1)\\ \cos(wt-4\pi/3+\phi_1)\end{bmatrix} + V^{-1}\begin{bmatrix}\cos(wt+\phi_{-1})\\ \cos(wt-4\pi/3+\phi_{-1})\\ \cos(wt-2\pi/3+\phi_{-1})\end{bmatrix} + V^{0}\begin{bmatrix}1\\1\\1\end{bmatrix} \tag{2.8}$$

Figure 2.9 shows the positive and negative sequence components in the alpha-beta frame. The positive sequence vector rotates in the positive direction while the negative sequence vector rotates in the negative direction.

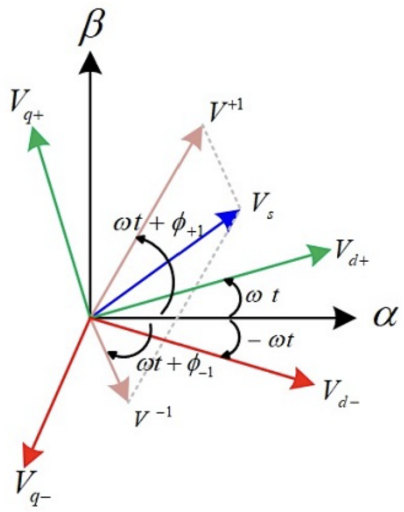

Figure 2.9: Positive and Negative sequence in alpha-beta frame

Taking the clark transform and ignoring the zero component and the zero sequence, we have:

$$V_{\alpha\beta} = V^{+1}\begin{bmatrix}\cos(\omega t+\phi_{+1})\\ \sin(\omega t+\phi_{+1})\end{bmatrix} + V^{-1}\begin{bmatrix}\cos(-\omega t+\phi_{-1})\\ \sin(-\omega t+\phi_{-1})\end{bmatrix} \tag{2.9}$$

If we take park transform and lock the angle by the positive sequence component, we have:

$$v_{dq+} = \left(V^{+1}\begin{bmatrix}\cos(\omega t+\phi_{+1})\\ \sin(\omega t+\phi_{+1})\end{bmatrix} + V^{-1}\begin{bmatrix}\cos(-\omega t+\phi_{-1})\\ \sin(-\omega t+\phi_{-1})\end{bmatrix}\right)\begin{bmatrix}\cos(\omega t) & \sin(\omega t)\\ -\sin(\omega t) & \cos(\omega t)\end{bmatrix} \tag{2.10}$$

By solving the above equation we can get the decoupled value of v_{dq+} as:

$$\begin{cases} v_{d+_{decoupled}} = V^{+1}\cos(\phi_{+1}) = v_{d+} - \bar{v}_{d-}\cos(2\omega t) - \bar{v}_{q-}\sin(2\omega t) \\ v_{q+_{decoupled}} = V^{+1}\sin(\phi_{+1}) = v_{q+} + \bar{v}_{d-}\sin(2\omega t) - \bar{v}_{q-}\cos(2\omega t) \end{cases} \tag{2.11}$$

Therefore, the block diagram of the DDSRF-PLL with decoupling network is shown in Figure 2.10.

The low pass filter (LPF) is used to eliminate the high frequency components in the decoupled voltage signals, which is the 2ω ripple. A common choice for the LPF is a first-order filter as:

$$G_{LPF}(s) = \frac{\omega_c}{s+\omega_c} \tag{2.12}$$

where ω_c is the cut-off frequency of the filter. The cut-off frequency should be chosen to be low enough to attenuate the 2ω ripple, but high enough to ensure a fast dynamic response of the PLL. A typical value for ω_c is around 30rad/s.

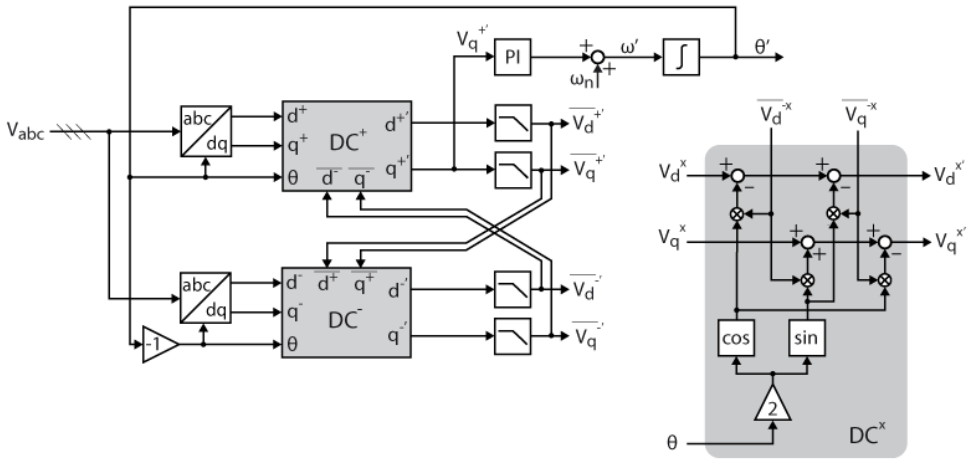

Figure 2.10: Block diagram of DDSRF-PLL with decoupling network

2.3.2 DDSRF-PLL under different grid conditions

To simply test the performance of the DDSRF-PLL under different grid conditions, a simulation is carried out in MATLAB/Simulink. The parameters of the DDSRF-PLL are chosen with a natural frequency of $\omega_n = 50Hz$ and a damping ratio of $\zeta = 0.707$. The cut-off frequency of the low pass filter is chosen to be $\omega_c = 30rad/s$.

The result of DDSRF-PLL under balanced grid conditions with a phase shift of $180°$ at $t = 0.1s$ is shown in Figure 2.11. It can be observed that the DDSRF-PLL can quickly track the phase angle of the grid voltage.

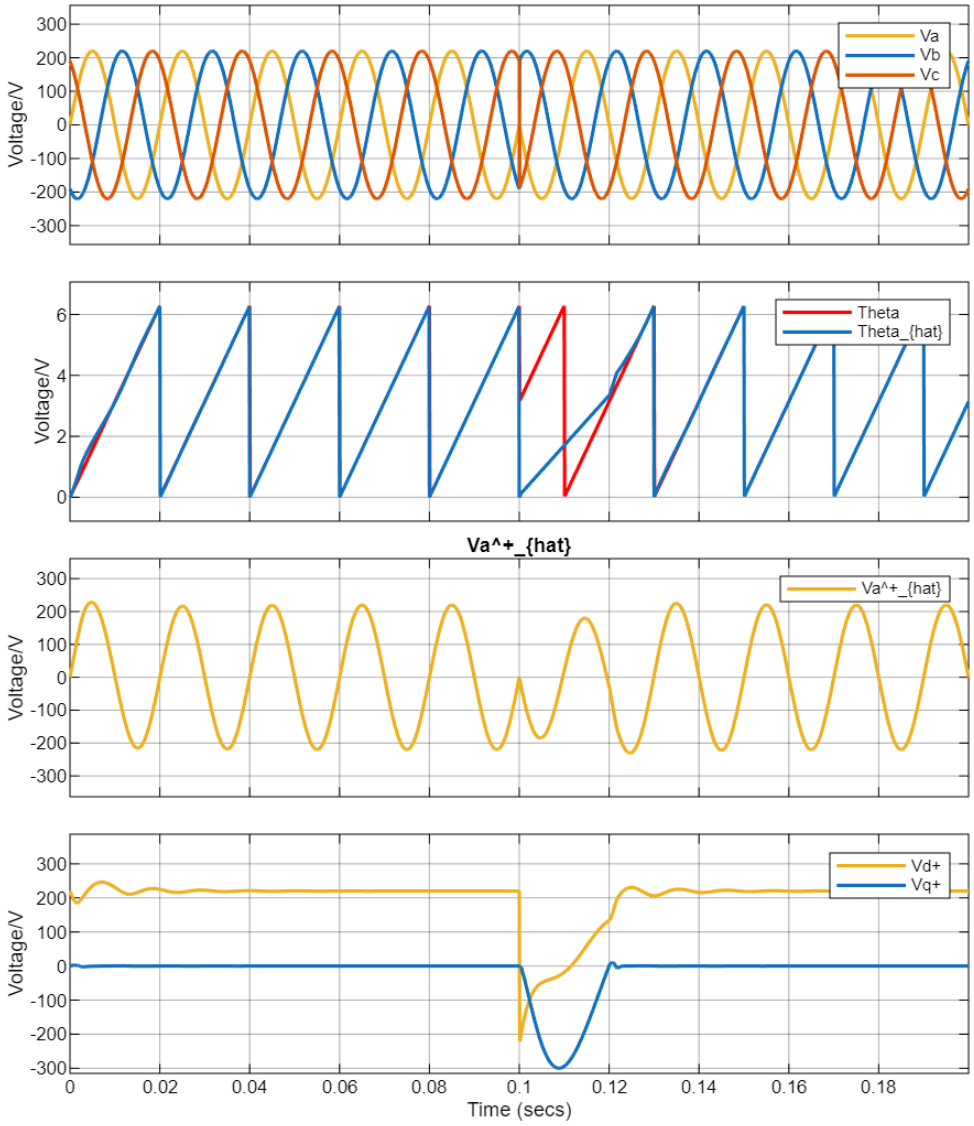

Figure 2.11: Response of the DDSRF-PLL with a phase shift at t=0.1s under balanced conditions. Utility voltage [V], Detected phase angle [rad], Fundamantal voltage [V] and SRF axes voltage [V]

The result of DDSRF-PLL under unbalanced grid conditions with a negative sequence component of 30% and a phase shift of $180°$ at $t = 0.1s$ is shown in Figure 2.12. It can be observed that the DDSRF-PLL can still track the phase angle of the grid voltage without any oscillations in the detected phase angle, thanks to the decoupling network that effectively separates the positive and negative sequence components. The d and q axis voltages also show no oscillations at twice the fundamental frequency, which indicates that the PLL is robust against unbalanced grid conditions.

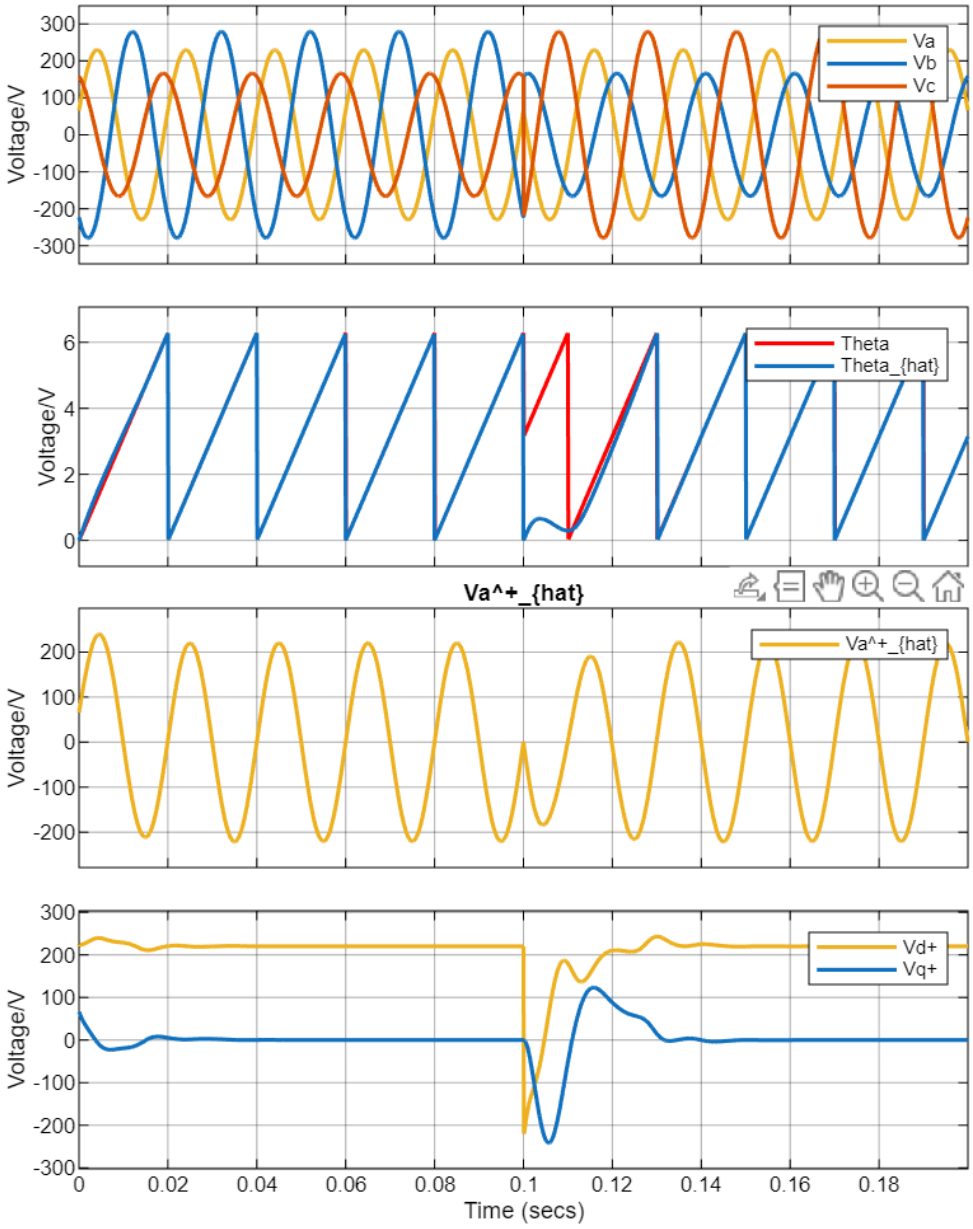

Figure 2.12: Response of the DDSRF-PLL with a phase shift at t=0.1s under unbalanced conditions. Utility voltage [V], Detected phase angle [rad], Fundamental voltage [V] and SRF axes voltage [V]

The result of DDSRF-PLL under grid conditions with 30% of the 5th harmonics and a phase shift of 180° at $t = 0.1s$ is shown in Figure 2.13. It can be observed that the DDSRF-PLL can still track the phase angle of the grid voltage without any oscillations in the detected phase angle, thanks to the decoupling network that effectively separates the positive and negative sequence components. The d and q axis voltages show oscillations at the harmonic frequencies, which indicates that teh DDSRF-PLL is still sensitive to harmonics in the grid voltage.

In conclusion, the DDSRF-PLL is an effective method for grid synchronization under unbalanced grid conditions. The decoupling network effectively separates the positive and negative

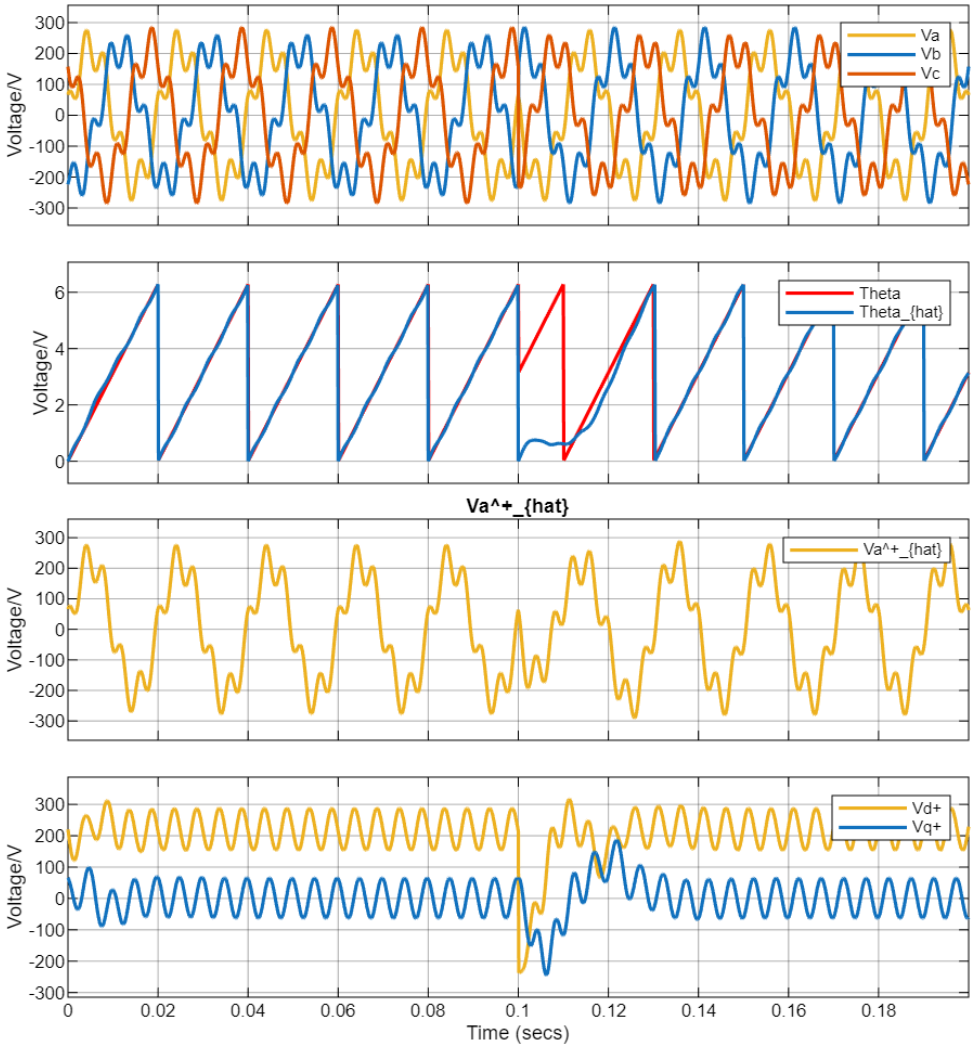

Figure 2.13: Response of the DDSRF-PLL with a phase shift at t=0.1s under grid conditions with 30% of the 5th harmonics. Utility voltage [V], Detected phase angle [rad], Fundamental voltage [V] and SRF axes voltage [V]

sequence components, ensuring accurate detection of the phase angle even under unbalanced voltages. However, the DDSRF-PLL is still sensitive to harmonics in the grid voltage, which can affect its performance. Therefore, for applications where the grid conditions are expected to be highly distorted, more advanced PLL techniques should be considered.

2.4 Second Order General Integrator PLL

2.4.1 SOGI-PLL concept

SOGI-PLL is proposed for use as phase detectors [3] and positive-sequence voltage extractors in single-phase grid-connected systems [4].

SOGI structures are mainly composed of two filter types. First, a band-pass filter with no

phase delay at the fundamental frequency is used for the estimation of the phase voltage v'. Secondly, a low-pass filter is used to obtain the in-quadrature component qv', which is $90°$ phase delayed from the input signal. Therefore, SOGI structures have the attractive benefit of providing simultaneous access to both the filtered output as well as a quadrature-shifted version of the same output, which represent the α and β components. As such, they allow for an easy implementation that can fit that of conventional SRF-PLL mentioned before.

The general principle of the SOGI-based PLL is given in Figure 2.14.

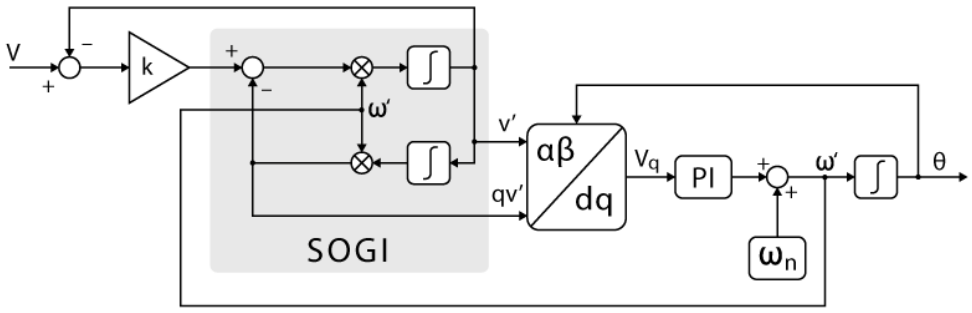

Figure 2.14: Block diagram of SOGI-PLL

Based on the preceding diagram, the subsequent transfer functions can be derived as follows:

$$D(s) = \frac{v'}{v}(s) = \frac{k\omega' s}{s^2 + k\omega' s + \omega'^2} \tag{2.13}$$

and the quadrature component is given by:

$$Q(s) = \frac{qv'}{v}(s) = \frac{k\omega'^2}{s^2 + k\omega' s + \omega'^2} \tag{2.14}$$

where ω' is the estimated angular frequency of the grid voltage, and k is the damping factor of the SOGI.

The effect of the damping factor k on the frequency response of the SOGI is shown in Figure 2.15.

An examination of the above transfer functions reveals that the parameter ω' centers the transfer function of the filters, while the parameter k plays a significant role in adjusting the filte's bandwidth.

It is also worth noting that the damping factor k does not alter the behavior of the SOGI at the frequency ω'. Consequently, a lower k value enhances frequency selectivity but slows down the response to voltage changes. Therefore, a trade-off between transient response and attenuation of distorsions must be made. A commonly adopted tuning is $k = \sqrt{2}$, which is equivalent to $k = 2\zeta = 2\frac{1}{\sqrt{2}}$, with ζ representing the damping ratio for a second-order system.

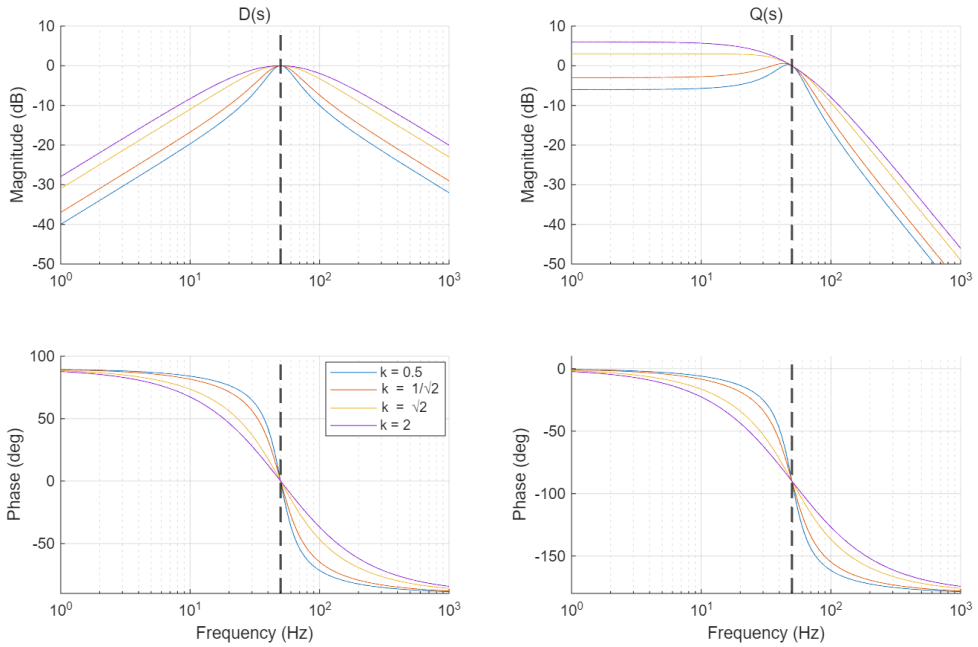

Figure 2.15: Effect of damping factor k on frequency response of SOGI

2.4.2 SOGI-PLL with DC offset rejection

In practical applications, the grid voltage may contain a DC offset component due to various reasons, such as sensor errors or power quality issues. If a DC offset is present in the measured voltage, it is not filtered by $Q(s)$ since the latter is of low-pass type. Consequently, the offset is also transferred to the quadrature signal and enters the SRF-PLL. This continuous term is then shifted to 2ω through the Park transformation, resulting in an oscillating term at twice the grid frequency in V_q. Given that the PI controller is unable to fully attenuate a non-continuous term, this oscillation is further propagated to the frequency and phase estimations.

To address this issue, a DC offset rejection technique can be implemented in the SOGI-PLL. SOGI block can be modified so that the low-pass filter generating the quadrature signal, $Q(s)$, is replaced with a band-pass filter with the same characteristics at the fundamental frequency. The block diagram of the SOGI-PLL with DC offset rejection is shown in Figure 2.16.

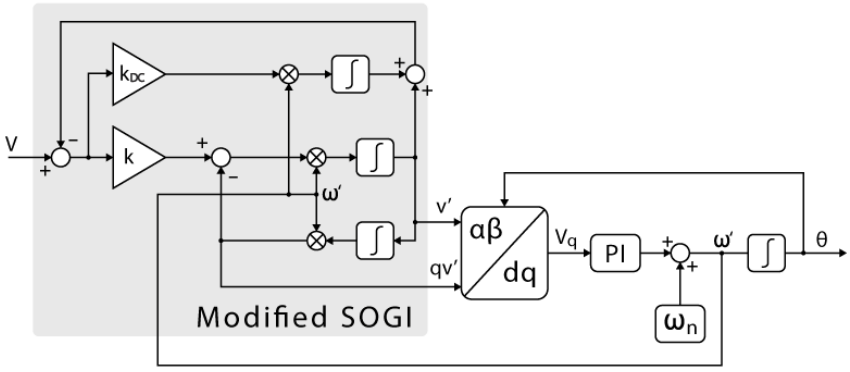

Figure 2.16: Block diagram of SOGI-PLL with DC offset rejection

The transfer function of the band-pass filter can be expressed as:

$$D(s) = \frac{v'}{v}(s) = \frac{k_{\text{dc}}\omega s^2}{s^3 + (k + k_{\text{dc}})\omega s^2 + \omega^2 s + k\omega^3} \tag{2.15}$$

$$Q(s) = \frac{qv'}{v}(s) = \frac{k_{\text{dc}}\omega^2 s}{s^3 + (k + k_{\text{dc}})\omega s^2 + \omega^2 s + k\omega^3} \tag{2.16}$$

The Bode diagram of the SOGI with DC offset rejection is shown in Figure 2.17.

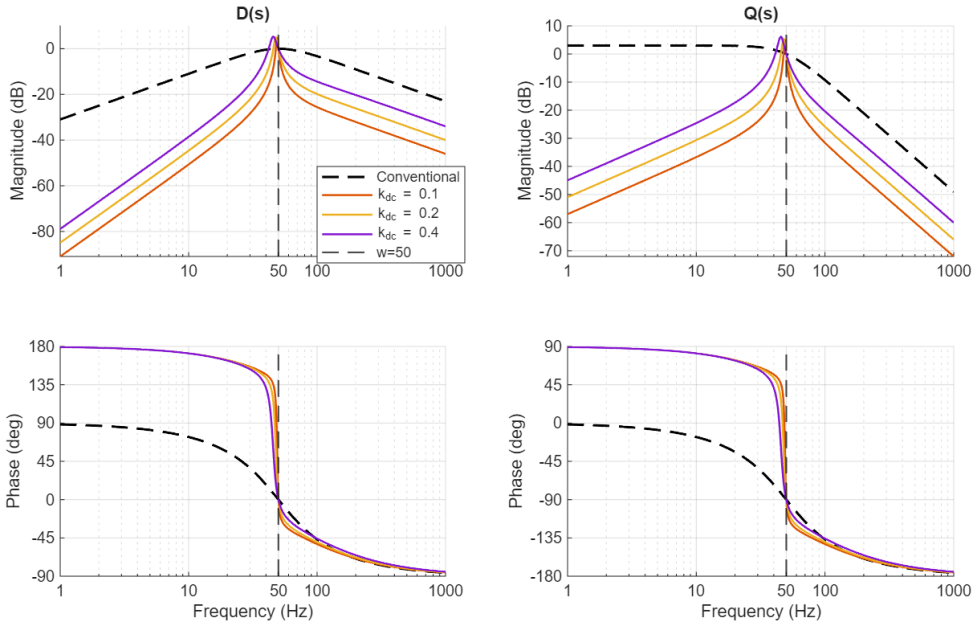

Figure 2.17: Bode diagram of SOGI with DC offset rejection

2.4.3 SOGI-PLL under different grid conditions

To simply test the performance of the SOGI-PLL under different grid conditions, a simulation is carried out in MATLAB/Simulink. The parameters of the SOGI-PLL are chosen with a natural frequency of $\omega_n = 50Hz$ and a damping ratio of $\zeta = 0.707$. The cut-off frequency of the low pass filter is chosen to be $\omega_c = 30rad/s$. The damping factor of the SOGI is chosen to be $k = \sqrt{2}$.

The result of SOGI-PLL without DC offset and harmonics with a phase shift of $180°$ at $t = 0.1s$ is shown in Figure 2.18. It can be observed that the SOGI-PLL can track the phase angle of the grid voltage, however the dynamic response is slower compared to the SRF-PLL and DDSRF-PLL.

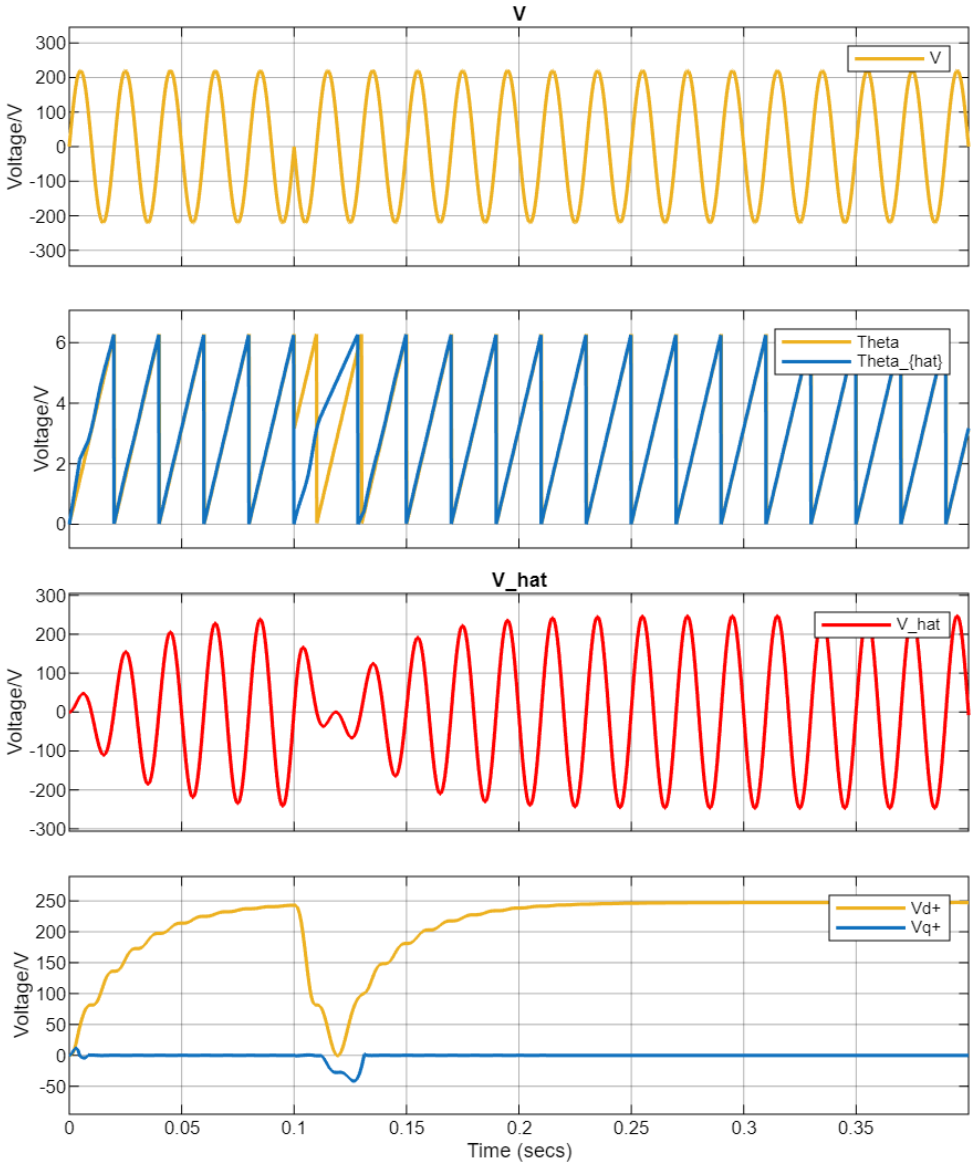

Figure 2.18: Response of the SOGI-PLL with a phase shift at t=0.1s without DC offset and harmonics. Utility voltage [V], Detected phase angle [rad], Fundamental voltage [V] and SRF axes voltage [V]

The result of SOGI-PLL with 66V DC offset and no harmonics with a phase shift of $180°$ at $t = 0.1s$ is shown in Figure 2.19. It can be obeserved that there is a slight oscillation in the detected phase angle due to the presence of DC offset in the grid voltage and a 2ω ripple in the d axis voltage. To solve this issue, the SOGI-PLL with DC offset rejection can be used as mentioned before.

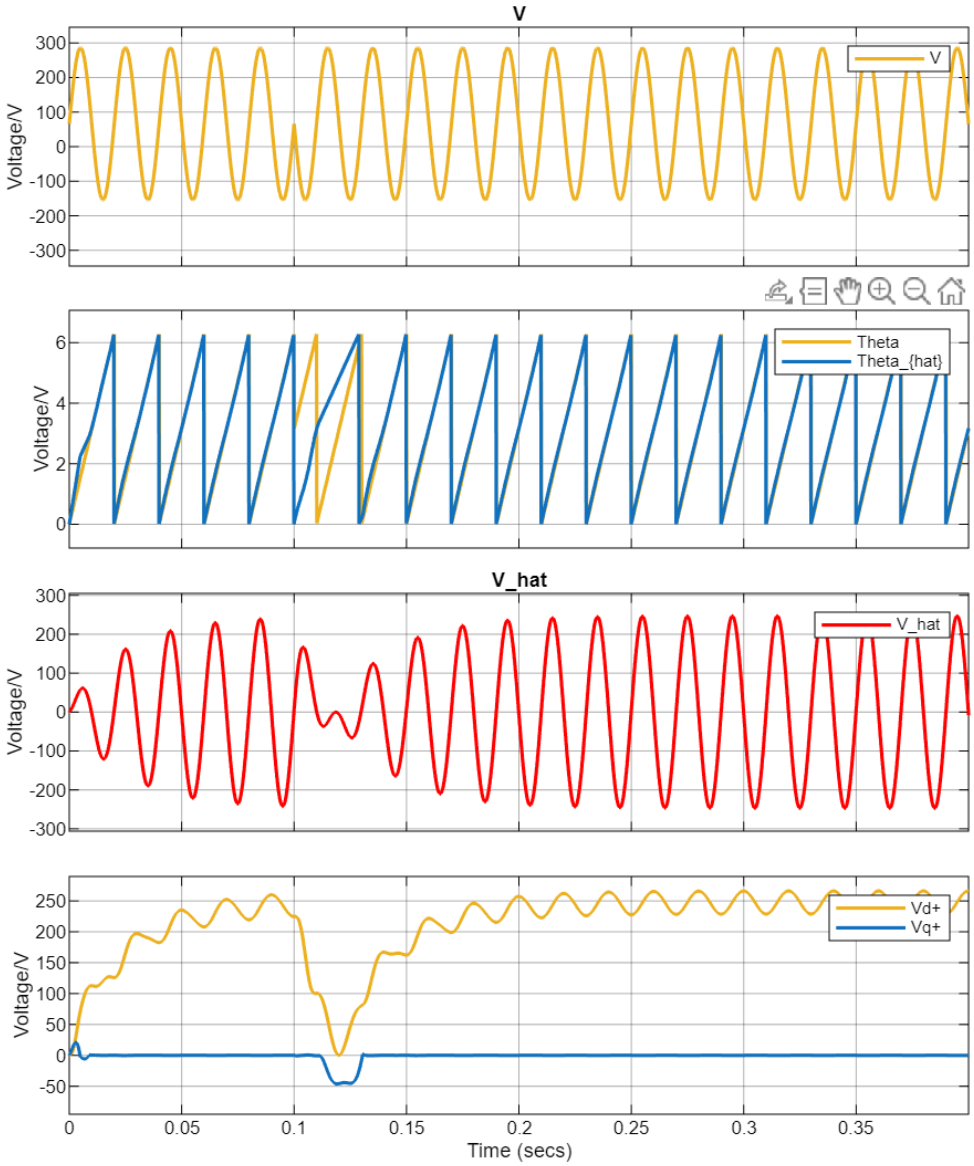

Figure 2.19: Response of the SOGI-PLL with a phase shift at t=0.1s with 66V DC offset and no harmonics. Utility voltage [V], Detected phase angle [rad], Fundamental voltage [V] and SRF axes voltage [V]

The result of SOGI-PLL with 30% of the 5th harmonics and no DC offset with a phase shift of $180°$ at $t = 0.1s$ is shown in Figure 2.20. It can be observed that the SOGI-PLL can still track the phase angle of the grid voltage without any oscillations in the detected phase angle, thanks to the SOGI structure that effectively filters out the harmonics. The d and q axis voltages show little oscillations at the harmonic frequencies, which indicates that the PLL is robust against harmonics in the grid voltage.

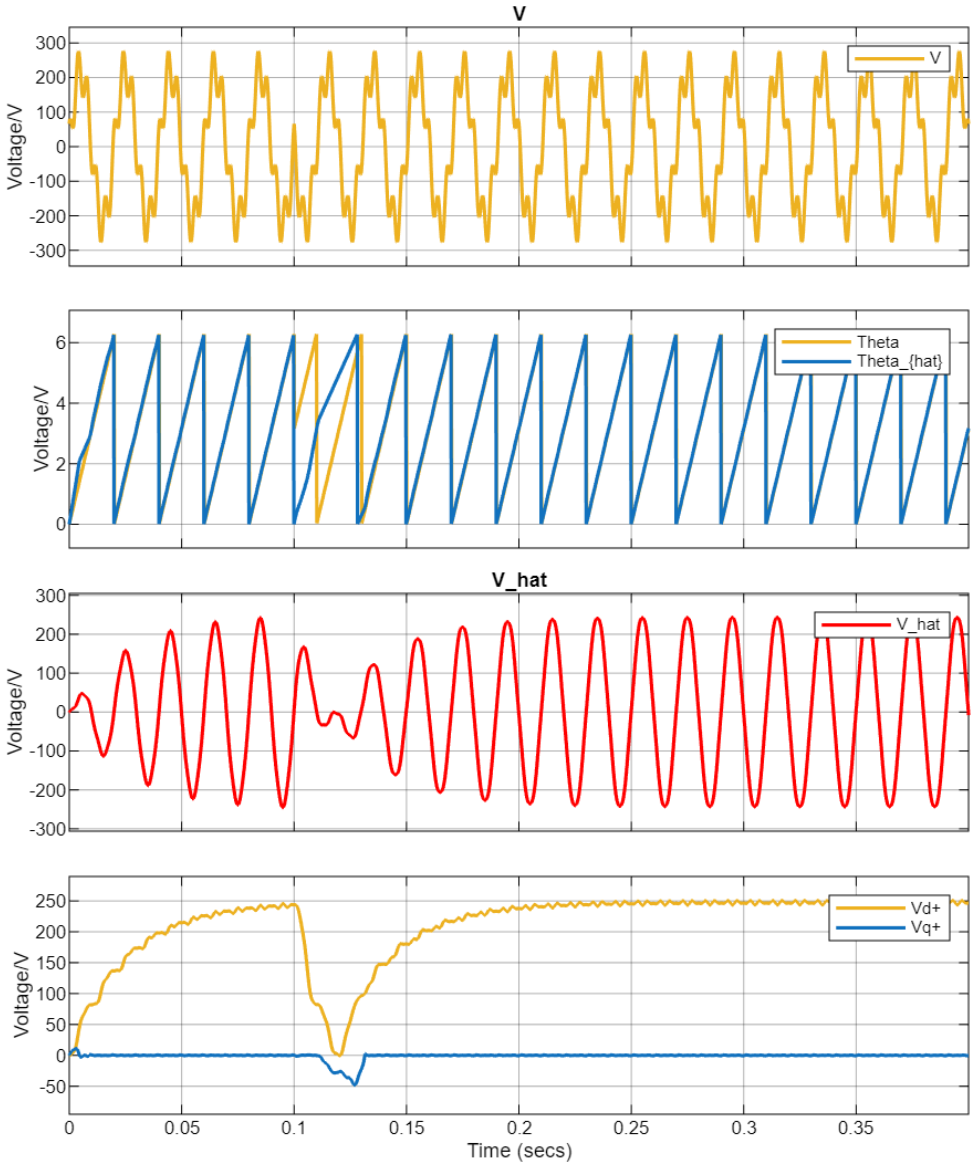

Figure 2.20: Response of the SOGI-PLL with a phase shift at t=0.1s with 30% of the 5th harmonics and no DC offset. Utility voltage [V], Detected phase angle [rad], Fundamental voltage [V] and SRF axes voltage [V]

2.4.4 Performance of SOGI-PLL with DC offset rejection

To simply test the performance of the SOGI-PLL with DC offset rejection under different grid conditions, a simulation is carried out in MATLAB/Simulink. The parameters of the SOGI-PLL with DC offset rejection are chosen with a natural frequency of $\omega_n = 50Hz$ and a damping ratio of $\zeta = 0.707$. The cut-off frequency of the low pass filter is chosen to be $\omega_c = 30rad/s$. The damping factor of the SOGI is chosen to be $k = \sqrt{2}$ and $k_{dc} = \sqrt{2}$.

The result of SOGI-PLL with DC offset rejection with 66V DC offset and no harmonics with a phase shift of $180°$ at $t = 0.1s$ is shown in Figure 2.21. It can be observed that the SOGI-PLL with DC offset rejection can track the phase angle of the grid voltage without any oscillations

in the detected phase angle, thanks to the band-pass filter that effectively filters out the DC offset. The d and q axis voltages show no oscillations at twice the fundamental frequency, which indicates that the PLL is robust against DC offset in the grid voltage. However, the dynamic response is still slower compared to conventional SOGI-PLL.

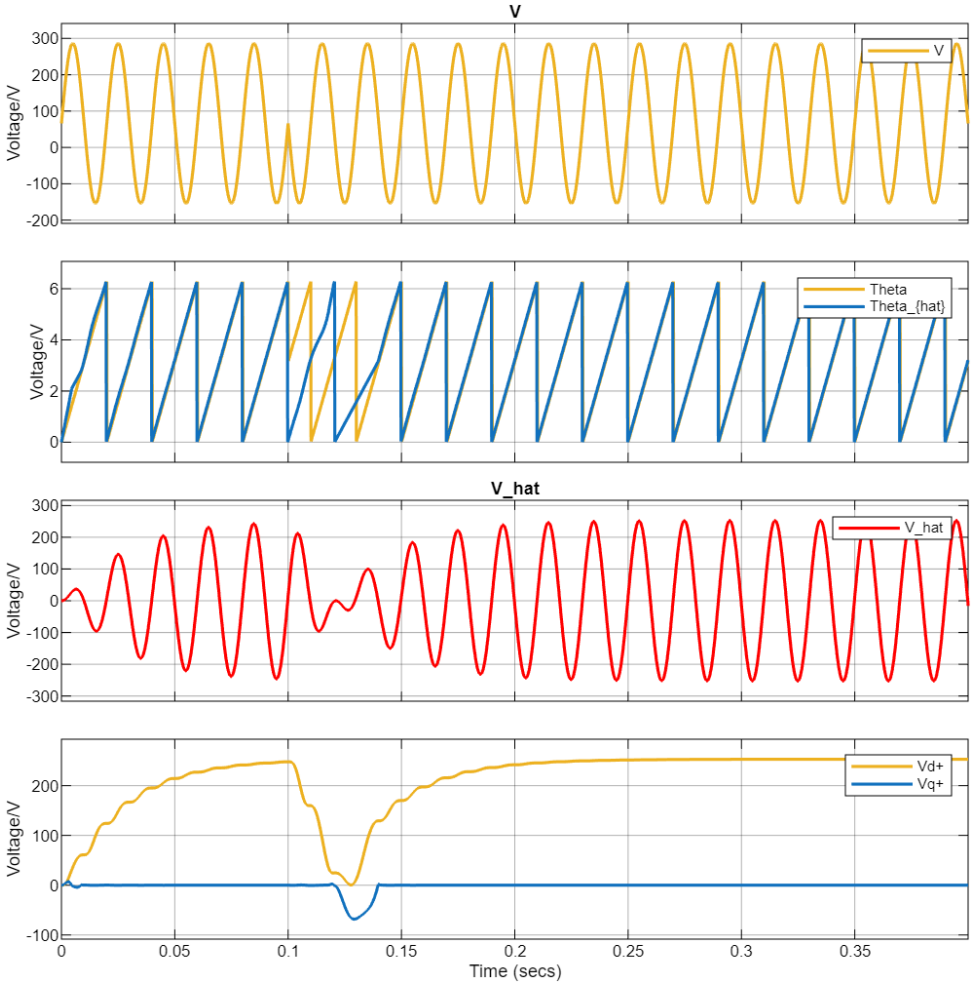

Figure 2.21: Response of the SOGI-PLL with DC offset rejection with a phase shift at t=0.1s with 66V DC offset and no harmonics. Utility voltage [V], Detected phase angle [rad], Fundamental voltage [V] and SRF axes voltage [V]

In conclusion, the SOGI-PLL is an effective method for single phase grid synchronization under distorted grid conditions. The SOGI structure effectively filters out harmonics in the grid voltage, ensuring accurate detection of the phase angle even under distorted voltages. However, the SOGI-PLL is sensitive to DC offset in the grid voltage, which can affect its performance. Therefore, for applications where the grid conditions are expected to have DC offset, the SOGI-PLL with DC offset rejection should be considered.

2.5 Dual Second Order General Integrator PLL

2.5.1 DSOGI-PLL concept

For three-phase synchronization systems, the DSOGI structure is common, since it not only attenuates low-order voltage harmonics but also allows ready estimation of symmetrical components by passing its output through a positive/negative sequence calculator (PSC) prior to feeding into the SRF-PLL. However, the estimated frequency from the SRF-PLL needs to be fed back into the SOGI to make it frequency adaptive, and thus provide accurate voltage magnitude and phase estimation as the grid frequency varies [5]. This feedback path limits the dynamic performance of the SRF-PLL, increases the complexity of tuning the PLL gains and reduces its stability margin [6].

The block diagram of the DSOGI-PLL is shown in Figure 2.22.

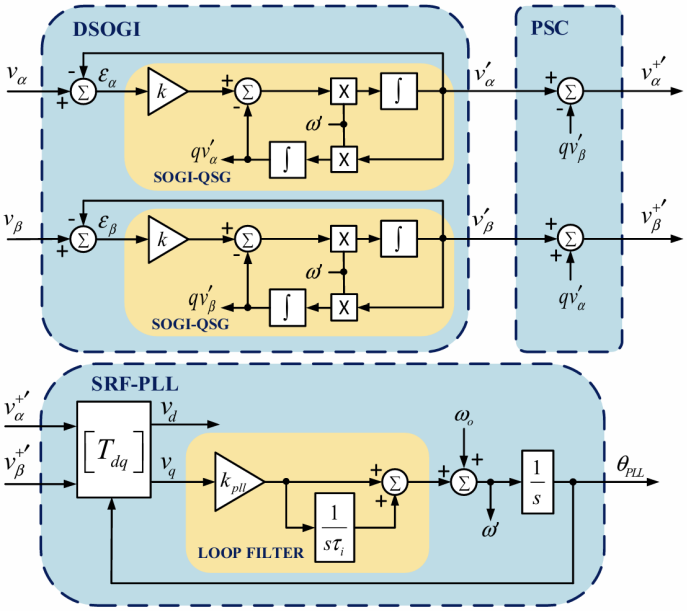

Figure 2.22: Block diagram of DSOGI-PLL

The DSOGI consists of two SOGIs, one for the α axis and one for the β axis. The transfer functions of the DSOGI can be expressed as:

$$\begin{aligned}\begin{bmatrix} v_\alpha^{+\prime}(s) \\ v_\beta^{+\prime}(s) \end{bmatrix} &= \frac{1}{2}\begin{bmatrix} D(s) & -Q(s) \\ Q(s) & D(s) \end{bmatrix}\begin{bmatrix} v_\alpha(s) \\ v_\beta(s) \end{bmatrix} \\ &= \frac{1}{2}\frac{k\omega}{s^2 + k\omega' + \omega'^2}\begin{bmatrix} s & -\omega' \\ \omega' & s \end{bmatrix}\begin{bmatrix} v_\alpha(s) \\ v_\beta(s) \end{bmatrix}\end{aligned} \tag{2.17}$$

The equation above shows how the combination of the DSOGI and the PSC form a low-pass filter that both filters out harmonic voltages and extracts the positive sequence only, from a distorted and unbalanced input voltage set. Consequently the positive sequence stationary frame

quadrature output signals $v_{\alpha}^{+'}$ and $v_{\beta}^{+'}(s)$ will have equal amplitudes, which will eliminate any unbalanced double frequency voltage oscillations prior to feeding the voltages into the SRF-PLL for phase angle and frequency estimation.

2.5.2 DSOGI-PLL under different grid conditions

To simply test the performance of the DSOGI-PLL under different grid conditions, a simulation is carried out in MATLAB/Simulink. The parameters of the DSOGI-PLL are chosen with a natural frequency of $\omega_n = 50Hz$ and a damping ratio of $\zeta = 0.707$. The cut-off frequency of the low pass filter is chosen to be $\omega_c = 30rad/s$. The damping factor of the SOGI is chosen to be $k = \sqrt{2}$.

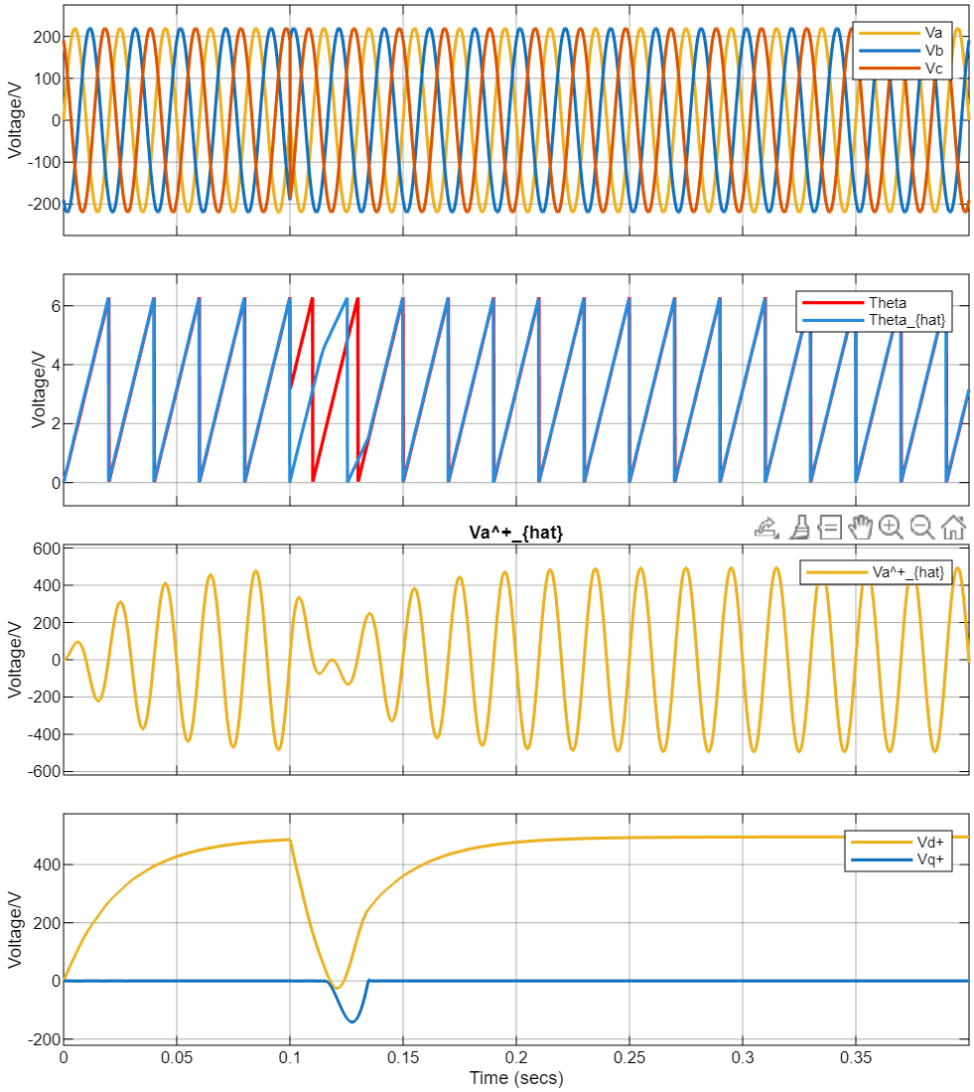

Figure 2.23: Response of the DSOGI-PLL with a phase shift at t=0.1s under balanced conditions. Utility voltage [V], Detected phase angle [rad], Fundamental voltage [V] and SRF axes voltage [V]

The result of DSOGI-PLL under balanced grid conditions with a phase shift of 180° at $t = 0.1s$ is shown in Figure 2.23. It can be observed that the DSOGI-PLL can quickly track the phase angle of the grid voltage.

The result of DSOGI-PLL under unbalanced grid conditions with a negative sequence component of 30% and a phase shift of 180° at $t = 0.1s$ is shown in Figure 2.24. It can be observed that the DSOGI-PLL can still track the phase angle of the grid voltage without any oscillations in the detected phase angle, thanks to the DSOGI structure that effectively filters out the negative sequence component. The d and q axis voltages also show no oscillations at twice the fundamental frequency, which indicates that the PLL is robust against unbalanced grid conditions.

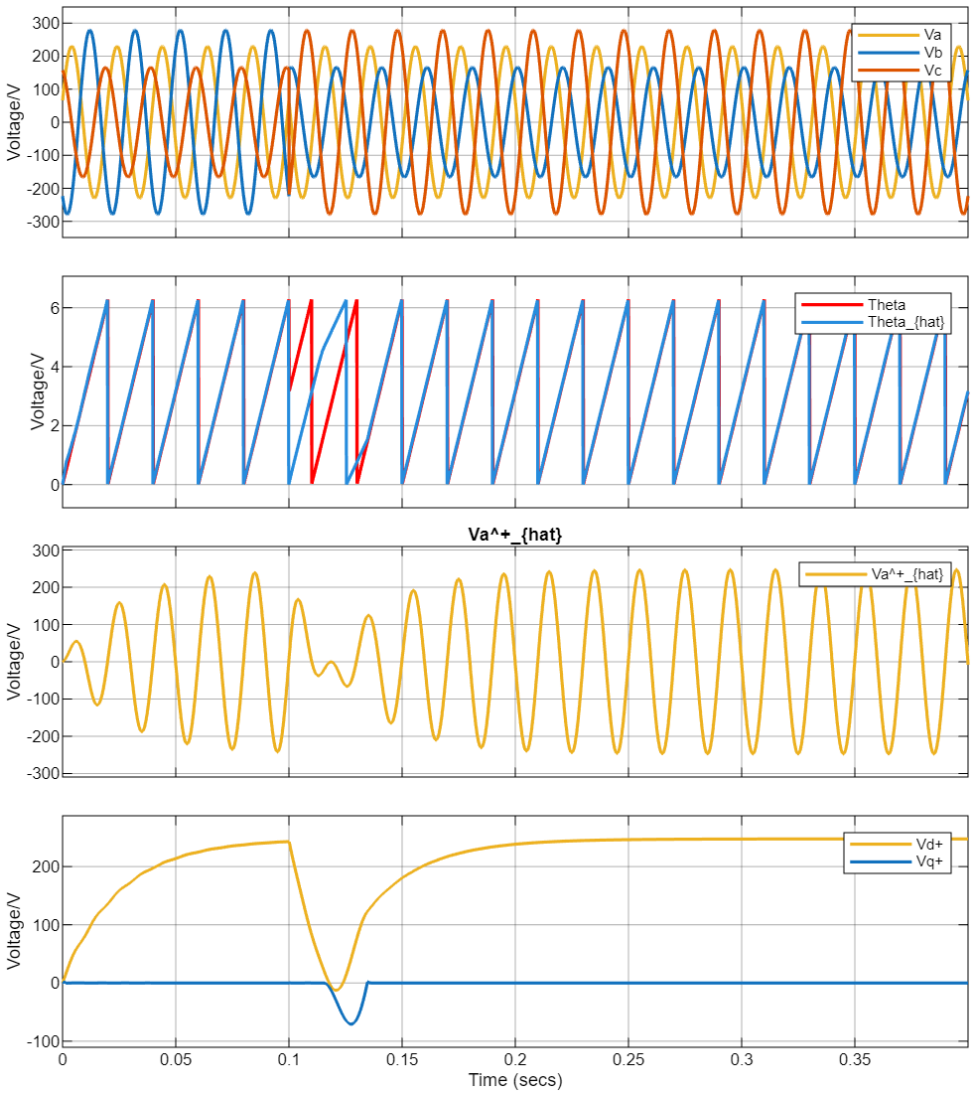

Figure 2.24: Response of the DSOGI-PLL with a phase shift at t=0.1s under unbalanced conditions. Utility voltage [V], Detected phase angle [rad], Fundamental voltage [V] and SRF axes voltage [V]

The result of DSOGI-PLL under grid conditions with 30% of the 5th harmonics and a phase

shift of $180°$ at $t = 0.1s$ is shown in Figure 2.25. It can be observed that the DSOGI-PLL can still track the phase angle of the grid voltage without any oscillations in the detected phase angle, thanks to the DSOGI structure that effectively filters out the harmonics. The d and q axis voltages show little oscillations at the harmonic frequencies, which indicates that the PLL is robust against harmonics in the grid voltage.

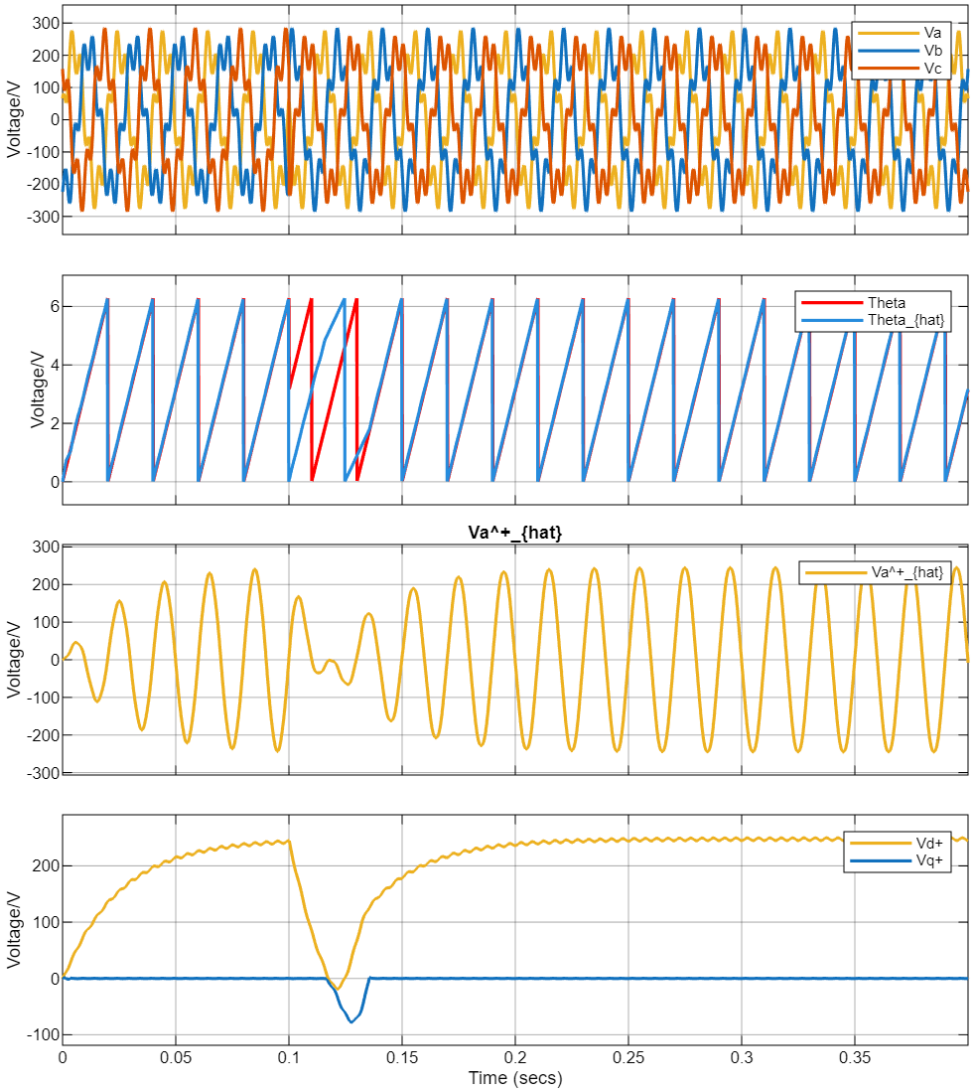

Figure 2.25: Response of the DSOGI-PLL with a phase shift at t=0.1s under grid conditions with 30% of the 5th harmonics. Utility voltage [V], Detected phase angle [rad], Fundamental voltage [V] and SRF axes voltage [V]

In conclusion, the DSOGI-PLL is an effective method for three phase grid synchronization under unbalanced and distorted grid conditions. The DSOGI structure effectively filters out negative sequence components and harmonics in the grid voltage, ensuring accurate detection of the phase angle even under unbalanced and distorted voltages.

2.6 Multiple Second Order General Integrator PLL

2.6.1 MSOGI-PLL concept

In a SOGI block, the attenuation of low-order harmonic distortions typically ranges between -10dB and -20dB for harmonics of order less than 10th when $k = \sqrt{2}$. However, in certain applications, this level of attenuation may prove insufficient. In order to selectively attenuate certain harmonics, a cross-feedback network composed of multiple SOGIs can be introduced, each tuned to the selected frequencies. This solution is referred to as the MSOGI-PLL. It is very effective for estimating the positive sequence component under disturbed conditions [7].

The block diagram of the MSOGI-PLL is shown in Figure 2.26.

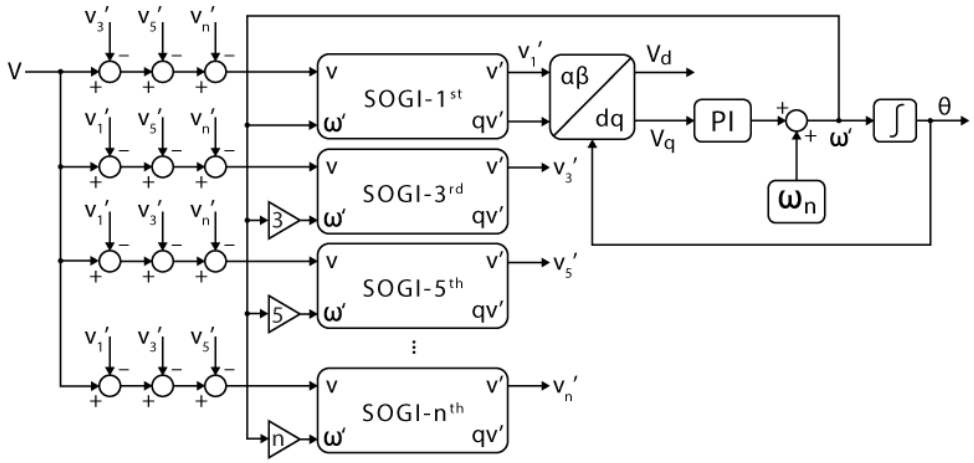

Figure 2.26: Block diagram of MSOGI-PLL

The parallel structure shown in Figure 2.26 forms a cross-feedback architecture often known as a Harmonic Decoupling Network (HDN). The key benefit of this network is that it creates sharp notches in the system's frequency response precisely at the frequencies where the individual SOGIs are tuned. As a consequence, the selective filtering characteristic of each SOGI is significantly improved. This enhancement allows the MSOGI-PLL to maintain a robust performance even in the presence of high distortion levels in the input signal.

The MSOGI consists of several SOGIs connected in parallel, each tuned to a specific harmonic frequency. The transfer function of the MSOGI can be expressed as:

$$v_i' = \left[D_i(s) \prod_{\substack{(j=1) \\ (j \neq i)}}^{n} \left(\frac{1 - D_j(s)}{1 - D_i(s) D_j(s)} \right) \right] v \tag{2.18}$$

where $D_i(s)$ represents the transfer function of the SOGI block tuned to the i-th harmonic frequency of interest.

2.6.2 MSOGI-PLL under different grid conditions

To simply test the performance of the MSOGI-PLL under different grid conditions, a simulation is carried out in MATLAB/Simulink. The parameters of the MSOGI-PLL are chosen with a

natural frequency of $\omega_n = 50Hz$ and a damping ratio of $\zeta = 0.707$. The cut-off frequency of the low pass filter is chosen to be $\omega_c = 30rad/s$. The damping factor of the SOGI is chosen to be $k = \sqrt{2}$. The MSOGI is designed to attenuate the 5th and 7th harmonics.

The result of MSOGI-PLL with 30% of the 5th and 7th harmonics and no DC offset with a phase shift of $180°$ at $t = 0.1s$ is shown in Figure 2.27. It can be observed that the MSOGI-PLL can track the phase angle of the grid voltage without any oscillations in the detected phase angle, thanks to the MSOGI structure that effectively filters out the 5th and 7th harmonics. The d and q axis voltages show little oscillations at the harmonic frequencies, which indicates that the PLL is robust against harmonics in the grid voltage.

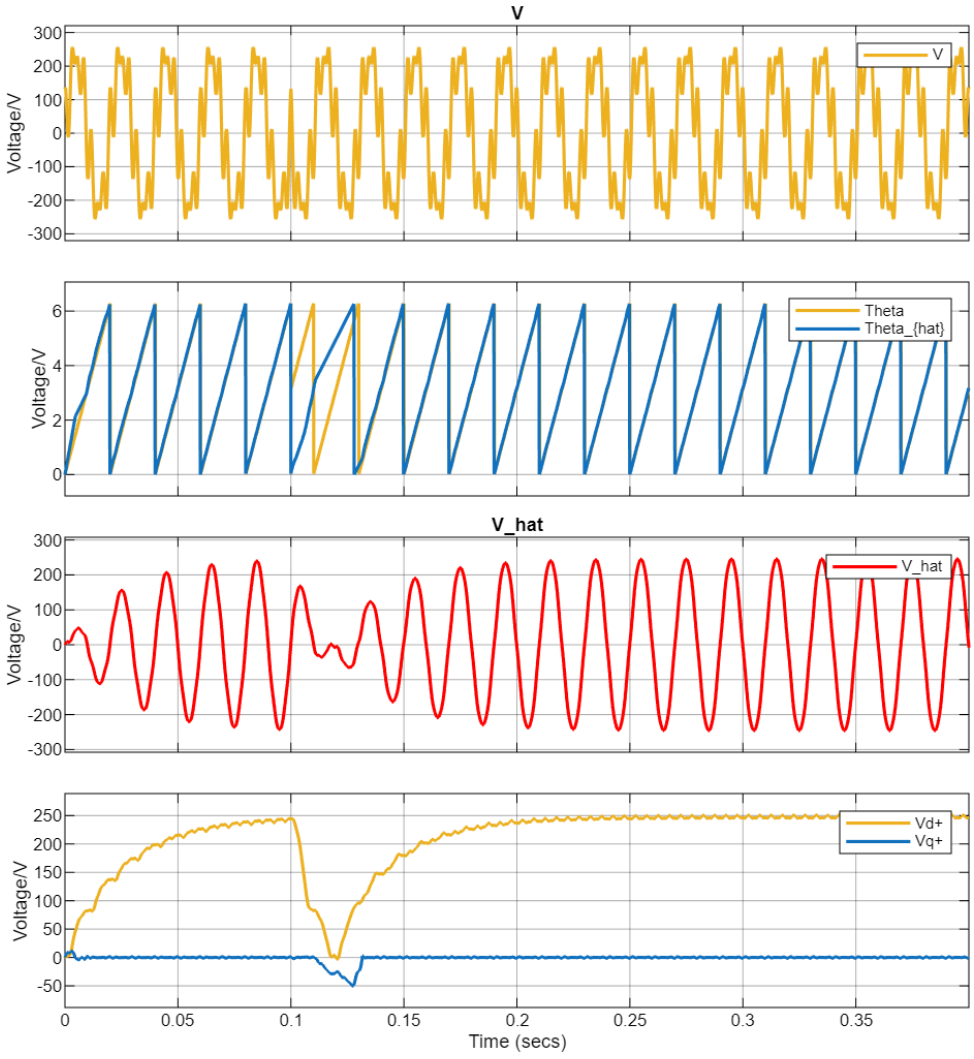

Figure 2.27: Response of the MSOGI-PLL with a phase shift at t=0.1s with 30% of the 5th and 7th harmonics and no DC offset. Utility voltage [V], Detected phase angle [rad], Fundamental voltage [V] and SRF axes voltage [V]

2.7 Comparison of PLLs

The following is a summerized description of the five different types of PLLs:

- SRF-PLL: Uses Park transformation to convert three-phase signals to d-q frame and locks the phase using PI control.
- DDSRF-PLL: An improved SRF-PLL that decouples positive and negative sequence components for better unbalance handling.
- SOGI: A second-order filter structure generating orthogonal signals from a single-phase input, used to extract fundamental frequency.
- DSOGI: Extension of SOGI for dual orthogonal outputs, positive and negative sequences in $\alpha - \beta$ frame.
- MSOGI: A bank of multiple SOGIs tuned to different harmonics; useful in harmonic estimation and multi-frequency systems.

For disturbances like unbalance, harmonics, and DC offset, the PLLs can be described in table 2.1.

Table 2.1: Comparison of Signal Disturbance Handling Capabilities

Technique	Unbalance Handling	Harmonics Immunity	DC Offset Immunity	Frequency Deviation Handling
SRF-PLL	Poor	Moderate	Poor	Good
DDSRF-PLL	Excellent	Moderate	Poor	Good
SOGI	Poor	Poor	Moderate	Moderate
DSOGI	Good	Moderate	Moderate	Good
MSOGI	Excellent	Excellent	Moderate	Excellent

Additionally, the dynamic response of the PLLs can be compared in table 2.2.

Table 2.2: Comparison of Dynamic Response

Technique	Dynamic Response
SRF-PLL	Fast
DDSRF-PLL	Moderate
SOGI	Slow
DSOGI	Moderate
MSOGI	Slow

The calculation time of the PLL is also an important factor to consider, especially in real-time applications. The computational complexity of each PLL can be summarized in table 2.3.

In summary, the choice of PLL technique depends on the specific application requirements, including the nature of the disturbances expected in the grid, the desired dynamic response, and the available computational resources. Each PLL has its strengths and weaknesses, and a careful evaluation is necessary to select the most suitable one for a given scenario.

Table 2.3: Comparison of Computational Complexity

Technique	Number of Operations	Memory Usage	Implementation Complexity
SRF-PLL	Low	Low	Low
DDSRF-PLL	High	Low	Moderate
SOGI	Moderate	Moderate	Moderate
DSOGI	High	Moderate	Moderate
MSOGI	High	High	High

CHAPTER 3

Further Guides for Your Report or Thesis

In the following, a few further guidelines (dos and don'ts) are given.

3.1 Guidelines for Your Presentation

3.1.1 Template, Software and Language

For an Engineer's Internship Report, Seminar Paper, Researcher's Report, Bachelor Thesis and Master Thesis you are invited to use this LaTeX template. You can also extract a few tips on writing in LaTeX (e.g. the tilde in `Fig.~\ref{key}` to avoid a line break).

LaTeX is highly (!) recommended, but any other software (e.g. Word, OpenOffice) may be used. TUM provides some templates (also for presentations) which may be used: `https://portal.mytum.de/corporatedesign`

English is preferred, but depending on the topic, German is also fine.

In any case, consult your supervisor for his/her specifications for your work.

3.1.2 Structure

A possible structure is given in the main part of this document. Generally, the motivation/introduction section usually has no subsections and may be up to two pages long (up to about three pages for a thesis). Limit the number of chapter levels/section levels (section, subsection, subsubsection) to three or four maximum.

If your topic is different from a controller design, the structure of your report/thesis can be different from the here proposed one. However, the abstract, the motivation/introduction and the conclusions and outlook sections remain as presented. For the structure of other topics of reports/theses, have a look into published papers with similar topics to yours. If your topic is a literature review, have a look e.g. in [8].

3.1.3 Page Count

For a bachelor or master thesis, the page count should be below 100 or maximum 150. In any case, be concise. Usually, it is not hard to write many pages, but to write few concise pages. It would be ideal if you can write as concise as 5 pages for a report or 50 pages for a thesis.

3.1.4 Style of Writing: Equations

It is a good style to handle any equation as part of a sentence. Instead of writing: "The gravitational force depends on the mass.

$$F = mg" \tag{3.1}$$

You should write: "The gravitation force depends on the mass and is given by

$$F = mg." \tag{3.2}$$

As the equation is at the end of the sentence, it ends with a period. Here is another example with an accessory sentence (usage of a comma in the equation): "The gravitational force is

$$F = mg, \tag{3.3}$$

where m is the mass."

Derive all your equations with symbols first. Afterwards and if appropriate, you can calculate numerical results or just list parameters and results in a table.

3.1.5 Style of Writing: Math Symbols

Use common math symbols and try to reduce the amount of used symbols if possible, but do not let room for ambiguity. A good practice is to write scalars normal s, vectors bold $\boldsymbol{v}$, matrices bold and capitalized $\boldsymbol{M}$ and nature constants normal and non-italic c. Use consistent multiplication symbols. A good practice is to use no multiplication symbol for variables, $F = mg$ and a centered dot for numbers, $F = 1\,\mathrm{kg} \cdot 9.81\,\mathrm{m/s^2}$. Do not use $F = 1\,\mathrm{kg} * 9.81\,\mathrm{m/s^2}$ or $F = 1\,\mathrm{kg} \times 9.81\,\mathrm{m/s^2}$ or $F = 1\,\mathrm{kg}.9.81\,\mathrm{m/s^2}$. These three symbols are reserved for convolution, cross product and point-separator. Function names are written normal, i.e. write $\sin(x)$ (i.e. `$\sin(x)$`) instead of $sin(x)$. You can also define your own function names with `$\operatorname{myFunc}(x)$` which becomes $\operatorname{myFunc}(x)$.

Every symbol needs to be explained at its first use, even if it is somewhat obvious such as mass m: The symbol m could have also been used for an amount as in $\sum_{i=1}^{m} x_i$.

Use appropriate braces in equations and make use of `\left` and `\right`.

3.1.6 Style of Writing: Braces and Footnotes

Reduce the usage of (braces) in the text and footnotes to a minimum. Either a statement is relevant and it could be in the normal text, or it is not so important and might be not written at all.

3.1.7 Style of Writing: Sentence Length, Adjectives, Superlatives, Assessments

Write short and concise sentences, best just in the form noun, verb, object, e.g. "Fig. x shows a block diagram of the controller." Avoid assessing adjectives/superlatives and the word "very", e.g. do not write "Kite power has enormous advantages and the proposed controller achieves a very high efficiency." Generally, only use statements that cannot be argued. The example sentence can be improved e.g. as follows: "Kite power has some advantages compared to conventional wind turbines, such as a lower material demand. The proposed controller achieved an efficiency of $x\,\%$." In that example, there is little to no room for arguments against the statements. You may let the reader assess your results, as in the last sentence of that example. Note that this is the difference of a scientific style of writing compared to the style usually used in marketing or journalism.

Before submitting a revision to your supervisor, it is a good idea to read your report/thesis aloud. Try to identify sentences, that can be shorter or divided into two (or more). Try to identify arguable statements, and remove them if they are not required. Find any other possibilities for improvements. Your goal is to submit a perfect report without any mistakes (in your eyes).

3.1.8 Style of Writing: Explanations

Write your findings/proposals as easy to read as possible. Write for someone who has not dealt in detail with your topic for months, but has a basic knowledge of your topic. For a controller implementation or a simulation model, it might be a good idea to ask yourself the following question: Is it possible to replicate your controller/model just with the information given in the text? For a thesis, you might give all the source codes and screenshots of simulation models, but already the mathematical equations and explanations should be enough for the reader to replicate your results. Generally it is a good idea to start your explanation/modeling with an axiom or with key assumption(s), e.g. "according to Newton's axioms, the dynamics of the kite is given by $\dot{\boldsymbol{p}} = \boldsymbol{F}_\Sigma, \dot{\boldsymbol{r}} = m^{-1}\boldsymbol{p}$, where ...", or for an electrical problem, "according to Kirchhoff's current law, the capacitor current is given by ..." Another start could be an equation based on conservation of power, energy or momentum. This is a point, where you can "pick up" an engineer/researcher of your field. From that point on, develop your model step-by-step. Use a similar step-by-step-approach for any other derivation such as your control method. You may also cite specific references to keep your derivation and page count short or to start your derivation from a more advanced "pick-up"-point. Your goal is to help the reader to understand your ideas and steps as easy as possible, without reading many other publications.

Write either in passive, e.g. "a current of $10\,\mathrm{A}$ was measured", or in the first person, e.g. "we/I measured a current of $10\,\mathrm{A}$". Use the present tense for explanations which have no time dependence, e.g. "the induced voltage is a function of the speed", and use the simple past tense for past actions, e.g. "the stability of the controller was proven" or "an efficiency of $x\,\%$ was measured". Other tenses are rare in a scientific report, see e.g. `https://www.ef.com/wwen/english-resources/english-grammar/verbs/` for the correct usage.

Use figures for your explanations. "An image can tell more than thousand words." Ideally, important parts of your mathematical derivation can be "seen" already in the figures, e.g. a vector diagram supports a trigonometric equation of your derivation. Create high quality vector

images e.g. with Inkscape and its LaTeX export and create plots e.g. with matlab2tikz or Pgfplots `https://de.overleaf.com/learn/latex/Pgfplots_package`. Tip: use your favorite search engine and look for "latex drawing software". Generally, labels should have the same (or similar) font and font size as the text of the template. It can take a lot of time to create a good/professional image or a good/professional plot, but it is worth it. A reader would usually first scan images, as they can summarize the most important parts of your work.

Push the figures/tables to appropriate locations in the text. A (sub)section title cannot be followed by a figure/table. Do not start a sentence with "But". Do not use short forms such as "can't" or "don't". Write it out, "cannot" and "do not".

3.1.9 Style of Writing: Paragraphs

Not every sentence is a paragraph, and a long section should have several paragraphs. Usually, the first sentence in a paragraph states a main point. Remaining sentences of the paragraph present information related to that main point.

3.1.10 Style of Writing: Abbreviations

Only use very common abbreviations, do not invent your own. Keep the usage of abbreviations at a minimum. A common abbreviation is PID controller which does not need further explanations. Another one would be PMSM for permanent magnet synchronous machine, which is often used by electrical engineers, but might be unknown by others. The first usage of such an abbreviation should be in the form "the abbreviation (TA)". Avoid abbreviations in the title of the report and in the abstract if possible.

3.1.11 Style of Writing: References, Citations

Reference to all figures and all tables at least once with "see Fig. x" and "see Tab. y" or "as shown in Figs. x–y" or similar (in LaTeX with `as shown in Figs.~\ref{tag1}-\ref{tag2}`). Reference equations with "solve (x) for m" (in LaTeX with `solve~\eqref{tag3} for $m$`).

Keep references to later sections of your report at a minimum, the only exception is the last part of the introduction to draw an outline. Do not write in future tense like "xy will be shown later". Also avoid to write "xy was shown in the equations earlier" or "above". Instead, always refer to specific sections, equations or figures.

Every statement or information from another source requires a reference to that source. This particularly also includes images. For images, the citation mark can be placed in the caption.

Do not start a sentence with a pure reference such as "(x) computes the force ..." or "[y] discussed MPC ...". Instead write "Eq. (x) computes the force ..." or "In [y] MPC was discussed ...". At the beginning of a sentence, you may also write out Equation, Figure or Table. In all other cases, use the short form Eq. (or just the equation number in braces, be consistent), Fig. or Tab. Do not alter the word for "Figure", i.e. do not write "see Image x" or "see Picture y". Always use "Fig. z". An equation number is always in braces, a reference is always in square braces and all other numbers are in no braces.

3.1.12 Style of Writing: Report Title

Keep the title short and concise. A good title is only one line, or maximum two lines. Do not use a title with more than three lines.

3.1.13 Style of Writing: Captions

Keep captions (e.g. of figures and tables) concise. They only describe what is shown. Discussions and interpretations are in the main text. The first letter of the first word of the caption is capitalized. The caption ends with a period.

3.1.14 Style of Writing: Lists

Lists should be used if appropriate. In a paper, you should use inline lists, e.g.: "The advantages of a PID controller are (i) the simplicity, (ii) the low computational demands and (iii) the stability." In a thesis, you might use bullet points instead. Each item should sound similar, i.e. if the first item starts with a noun, all other items should also start with a noun. If the first item is a sentence, all other items should be a sentence, etc.

3.1.15 Spelling

Before you submit a revision to your supervisor, always use a spell checker for the complete document. Check for the correct use of "a", "an", "the" and plural.

3.1.16 Quotation Marks in LaTeX

The quotation mark symbol in LaTeX is not `"`. It is `` `quoted' `` or the respective UTF-8 symbols "quoted" (you might have shortcuts on your operating system).

Use bibtex (or alternatively biber) for the bibliography in LaTeX. For many publication databases you find the bibtex entry of a paper online (e.g. google books or IEEExplore) which just needs to be copied and pasted into your bib file: Fig. 3.1 shows a screenshot from IEEExplore. After clicking on "Download Citation", copy the text and paste it into your ".bib" file.

3.1.17 Further Reading

Please also read "How to write for Technical Periodicals & conferences" by IEEE, `https://journals.ieeeauthorcenter.ieee.org/wp-content/uploads/sites/7/How-to-Write-for-Technical-Periodicals-and-Conferences.pdf`, at least Secs. 6–7. Another guide is `http://journals.aps.org/files/rmpguide.pdf`.

3.2 Guidelines for Your Presentation

In the following, a few guidelines (dos and don'ts) for your presentations are given:

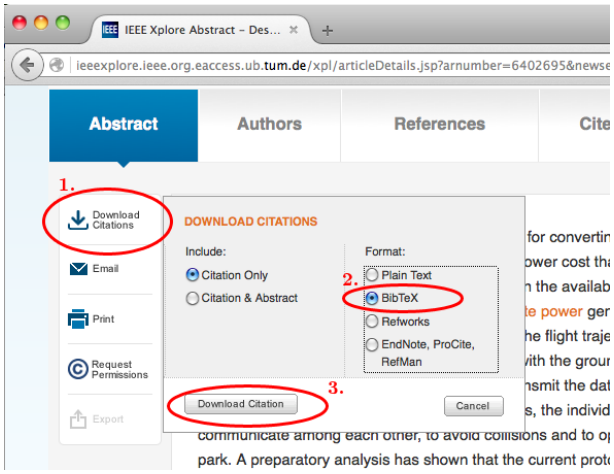

Figure 3.1: Downloading a bibtex entry from IEEExplore.

- Do not create a bullet point-"standard" Power Point presentation.
- Place almost no math on the slides, except one can understand quickly, and if it helps to illustrate your idea.
- Instead, use images and graphs, with which you tell a story and sketch your idea. A story teller does not need to draw an outline at the beginning of the story.
- Place affiliation, dates, logos etc. only on the first slide (title slide). On all other slides, place only a slide number and do note place other boarders. Use a single color background, e.g. just black or white.
- Do not overload your slides.
- Use a similar structure as in your report/thesis: title, motivation incl. previous/related works, your approach/idea, your results, conclusions, outlook.
- Rehearse your presentation several times. Make sure, you are $\pm 3\,\mathrm{min}$ maximum within the set time limit. You usually need about $1\,\mathrm{min}$ per slide.
- Create your presentation with only one target: The audience shall understand your key idea. Mathematical details etc. can be found in your report/thesis.

CHAPTER 4

Conclusion

An example for conclusion chapter.

4.1 Summary

The goals of this work were

1. to find solutions to reduce the calculation effort for FS-MPC methods,
2. to increase the time resolution of FS-MPC methods in order to reduce ripples on the controlled variables and
3. a combination of the two last points, i.e. to find methods to reduce ripples on the controlled variables with less calculation effort.

Within this work solutions for all three items have been proposed and were proven experimentally.

It was also verified that FS-MPC methods offer several advantages over conventional PID controllers:

1. Multivariable control is easily possible (control of two currents, both flux and torque, and also the voltage balancing can be performed by one single FS-MPC controller).
2. Constraints can be considered without problems and nonlinearities can also be included.
3. FS-MPC controllers can easily operate the system at its physical limits. Conventional controllers mostly need additional (adaptive) schemes and feed forward controllers to achieve the same or similar dynamics.
4. FS-MPC controllers do normally not produce an overshoot which is usual for conventional controllers.

4.2 Final evaluation

As already mentioned, the applicability of direct switching strategies is highly dependent on the power range of the system: For medium- and high-voltage systems the system losses are dominated by the inverter switching losses. In this case switching frequencies of only a few hundred Hz per device are desired. For that reason industrial applications of FS-MPC methods have been reported mainly for high-power systems (MPDTC which was developed by ABB). Compared to classical DTC, MPDTC can lead to a further reduction of the switching frequency while maintaining at the same time the same quality of the control result. Sophisticated FS-MPC methods can partly even outperform Optimized Pulse Patterns for these types of drive systems [9].

In contrast to this, the presented work deals with low-voltage and smaller systems which are in the range of a few kW. For these applications a good quality of the controlled variables is usually much more important than a low switching frequency as in this case the inverter losses are less dominant. For these applications switching frequencies of 10–$20\,\mathrm{kHz}$ per device can be easily handled. The conventional FS-MPC approach only allows to change an inverter switching state at the *beginning* of a sample which is the reason for undesired high ripples. Another very important drawback of FS-MPC is the high calculation effort which rises exponentially with the prediction horizon. Thus, in this work several extensions to FS-MPC in order to reduce the calculation effort and to reduce ripples on the controlled variables were presented. As the shown experimental results clearly verify, the proposed extensions can effectively reduce these two drawbacks of FS-MPC methods. These extensions could even be successfully implemented for more sophisticated inverter topologies (three-level NPC and FC) where several tasks have to be performed by one single FS-MPC (e.g. control of two currents and three FC voltages). Even despite the high number of possible switching states (27 for an NPC and 64 for an FC inverter), up to three prediction steps could be realized in real-time with sampling rates up to $16\,\mathrm{kHz}$. For the proposed methods only one or two weighting factors have to be tuned (if any at all). Compared to linear controllers where parameter tuning is a work-intensive and crucial task, the proposed algorithms just need to be implemented and the weighting factors can be tuned quickly.

Although the methods presented within this work can enable FS-MPC strategies to become more attractive also for smaller and low-power (drive) systems, it is still questionable whether FS-MPC can outperform PWM-based MPC methods: For continuous-valued optimization tasks and linear systems the optimization problem can be solved analytically (e.g. with the MPT toolbox) which drastically reduces the calculation effort. PWM distributes the switching time points over the whole sample which leads to excellent control results in terms of ripples. Compared to the calculation of a VSP or to the implementation of an oversampled FS-MPC in hardware, the basic idea of PWM is ingeniously simple and has been proven to work well within the last decades. For multilevel inverters it is also possible to include a voltage balancing algorithm into the PWM which means that the overlaying controller only needs to calculate the voltages which should be applied—then it is not necessary to handle the voltage balancing within the control algorithm itself. Another drawback of FS-MPC is the varying switching frequency: Compared to PWM, FS-MPC methods produce an undesired audible noise which is much more annoying than the sound of PWM. Of course, it is also possible to modify the cost function such that a more or less constant switching frequency per device can be obtained. However, this can only be achieved at the expense of a deteriorated result regarding the main control objective (to mini-

mize the control deviation). Thus, in order to achieve the same control result in terms of ripples as without forcing a constant switching frequency, the sampling frequency and with it the time resolution of FS-MPC has to be drastically increased.

4.3 Outlook

There are several possibilities to extend and to modify the strategies which were presented in this work: One promising extension could be a method to calculate not only one but two or even more VSPs. If e.g. only one IGBT is allowed to switch at a time and if two VSPs are calculated within one sample, "online optimized" pulse patterns and a constant switching frequency could be obtained. Such an FS-MPC method would then be fully comparable to PWM in terms of ripples on the controlled variables. Another possibility would also be to increase the prediction horizon for VSP methods.

Another very promising application for (FS-)MPC is to perform direct speed or even position control for electrical drives. In this way all disadvantages which result from cascaded control loops could be overcome. Furthermore, it would then also be possible to operate the drive at its physical limits while still keeping all controlled variables within their allowed range.

APPENDIX A

List of symbols and abbreviations

A.1 List of symbols

General remark:
The following convention was used for variables:

Scalars are italic letters:	x
Vectors are bold lower case letters:	$\boldsymbol{x}$
Matrices are bold upper case letters:	$\boldsymbol{X}$
References are marked with a star superscript:	x^*

Used symbols:
In the following the most important symbols are listed which are used within this work.

General symbols:

$\boldsymbol{x}$	State vector
$\boldsymbol{u}$	Input vector
$\boldsymbol{y}$	Output vector
$\boldsymbol{A}$	State matrix
$\boldsymbol{B}$	Input matrix
$\boldsymbol{C}$	Output matrix
$\boldsymbol{D}$	Feedthrough matrix
t	Time (continuous)
k	Time (discrete, current sample)
$\frac{\mathrm{d}}{\mathrm{d}t}$	Time derivation
T_s	Sampling time
t_sw	Variable switching time point (VSP)
Δ	Difference
J	Inertia

General electrical variables:

a, b, c	Phases
α, β	Equivalent two-phase coordinates
j	$\sqrt{-1}$
v	Voltage
i	Current
R	Resistor
C	Capacitor
L	Inductor

Induction machine parameters:

$\boldsymbol{v}_\mathrm{s}$, $\boldsymbol{v}_\mathrm{r}$	Stator and rotor voltage
$\boldsymbol{i}_\mathrm{s}$, $\boldsymbol{i}_\mathrm{r}$	Stator and rotor current
$\boldsymbol{\psi}_\mathrm{s}$, $\boldsymbol{\psi}_\mathrm{r}$	Stator and rotor flux
ω_m	Mechanical machine speed
ω_el	Electrical machine speed
T_m	Mechanical machine torque
T_l	Mechanical load torque
P	Machine power
p	Number of pole pairs
R_s, R_r	Stator and rotor resistance
L_s, L_r	Stator and rotor inductance
L_m	Mutual inductance

Further variables and parameters:

S_{xi}	Switch i in phase x
s_{xi}	Gating signal for switch i in phase x
j	Cost function value
w	Weighting factor
v_o, i_o	Inverter output voltage and current (UPS)
v_l, i_l	LC lowpass-filter output voltage and current (UPS)

A.2 List of abbreviations

AC	Alternating Current
AD	Analog to Digital (converter)
CPLD	Complex Programmable Logic Device
CPU	Central Processing Unit
DA	Digital to Analog (converter)
DC	Direct Current
DMTC	Direct Mean Torque Control
DSC	Direct Self Control
DSP	Digital Signal Processor
DTC	Direct Torque Control
EMI	Electromagnetic Interference
FC	Flying Capacitor
FIFO	First In First Out (buffer)
FOC	Field Oriented Control
FPGA	Field Programmable Gate Array
FS	Finite-Set
FS-MPC	Finite-Set Model Predictive Control
GPC	Generalized Predictive Control
HDL	Hardware Description Language
IGBT	Insulated Gate Bipolar Transistor
IM	Induction Machine, Induction Motor
ISA	Industry Standard Architecture (bus)
LCD	Liquid Crystal Display
LP	Linear Program
LTI	Linear Time-Invariant
MILP	Mixed Integer Linear Program
MIQP	Mixed Integer Quadratic Program
MPC	Model Predictive Control
MPDTC	Model Predictive Direct Torque Control
mpLP	Multiparametric Linear Program
mpQP	Multiparametric Quadratic Program
MPT	Multiparametric Toolbox
NP	Neutral Point
NPC	Neutral Point Clamped
PCC	Predictive Current Control
PTC	Predictive Torque Control
PWM	Pulse Width Modulation
QP	Quadratic Program
RAM	Random Access Memory
RMS	Root Mean Square
RPM	Revolutions Per Minute
RTAI	Real-Time Application Interface

SI	International System of Units
SVM	Space Vector Modulation
THD	Total Harmonic Distortion
UPS	Uninterruptible Power Supply
VHDL	Very High Speed Integrated Circuit Hardware Description Language
VSP	Variable Switching Point
VSP2CC	Variable Switching Point Predictive Current Control
VSP2TC	Variable Switching Point Predictive Torque Control

APPENDIX B

Test bench data

B.1 Two-level inverter test bench

A quick overview of the two-level inverter test bench has already been given in chapter X. The complete test bench consists of a real-time computer system, two squirrel-cage induction motors, two two-level inverters and measurement devices. It is to be noted that for this test bench no DC link voltage measurement is possible.

B.1.1 Real-time computer system

The real-time computer system consists of a PC104 module with a 1.4 GHz Pentium M CPU, 1 GB RAM and a 60 GB hard disk. All components are mounted into a 19 inch rack. The system is running an Arch Linux distribution with an RTAI (real-time application interface) kernel patch. This RTAI kernel patch allows to program kernel modules which can be executed in real-time. The real-time control algorithm can be conveniently programmed in *C*.

The necessary peripheral hardware for analog and digital in- and outputs is connected via the 16 bit ISA bus. The used 19 inch rack has space for up to twelve extension boards. In order to measure the signal from the current transducers, an AD card with two channels is used. The encoder signal can be read via a special encoder board. The most important extension card is responsible for the inverter gating (PWM) signals: In order to synchronize the generation of these gating signals with the control algorithm which is running on the real-time computer, this card also generates an interrupt for the real-time computer. Every time when such an interrupt occurs, the control algorithm is executed. Thus, the whole control algorithm is triggered by this extension card. As this board contains an FPGA, it is possible to modify the existing implementations for the generation of the gating signals according to the user's needs. The current implementation allows of course the generation of PWM signals but direct switching and switching at a VSP is also possible. Furthermore, the interrupt for the control algorithm also triggers the measurements of the AD converters such that it is possible to trigger the measure-

ments at the beginning of a sample. In order to conveniently output measured values, DA cards can be inserted into the system as well: Then, variables can be easily visualized and recorded with an oscilloscope. Another extension board with a four digit hexadecimal (16 bit) display and four hexadecimal switches can be used for status notifications and user interaction (start and stop of the control algorithm, reference value changes etc.). Further information about this system can be found in [10].

B.1.2 Inverters

As already mentioned, the test bench consists of two inverters. Both inverters are supplied from a three-phase voltage source with an RMS phase to phase voltage of $400\,\mathrm{V}$. Since the inverters cannot feed back energy to the three-phase grid, the DC link voltage will rise if a connected machine is operated in generator mode. In order to avoid damages of the system, a break chopper resistor can be connected to discharge the DC link such that the voltage level does not become critical. Since both machines are connected to each other, one drive is normally operated as motor while the other one works as generator. Thus, in order to avoid a frequent use of the break chopper resistor, the DC links of both drives are coupled together.

The controlled inverter is a modified Seidel/Kollmorgen Servostar 600 $14\,\mathrm{kVA}$ inverter. It allows the user to directly command the IGBT gating signals from the real-time computer system. This inverter is connected to the working machine which is also controlled by the user. Consequently, the load inverter (Danfoss VLT FC-302 $3.0\,\mathrm{kW}$) is connected to the load machine. This inverter allows to perform speed and torque control of different machines. Furthermore, it can also be used to measure machine parameters.

B.1.3 Induction machines

Table B.1: Parameters for the working machine of the two-level inverter test bench

Parameter	Value
Nominal power P_{nom}	$2.2\,\mathrm{kW}$
Synchronous frequency f_{syn}	$50\,\mathrm{Hz}$
Nominal current $\lvert\boldsymbol{i}_{\mathrm{s,\,nom}}\rvert$	$8.02\,\mathrm{A}$
Power factor $\cos(\varphi)$	0.85
Nominal speed ω_{nom}	$2772\,\mathrm{rpm}$
Number of pole pairs p	1
Stator resistance R_{s}	$2.6827\,\Omega$
Rotor resistance R_{r}	$2.1290\,\Omega$
Stator inductance L_{s}	$283.4\,\mathrm{mH}$
Rotor inductance L_{r}	$283.4\,\mathrm{mH}$
Mutual inductance L_{m}	$275.1\,\mathrm{mH}$
Inertia J	$0.005\,\mathrm{kg\,m^2}$

The two-level inverter test bench consists of two $2.2\,\mathrm{kW}$ squirrel-cage induction machines which are coupled to each other. The parameters of the working machine (driven by the controlled inverter) are given in Table B.1. The load machine is completeley operated by the load inverter and hence, its parameters are not shown. The parameters were measured with the Danfoss load inverter. On both machines incremental encoders with 1024 points are mounted.

B.2 FPGA-based test bench

In chapter X a quick overview of the FPGA-based test bench has already been given. It consists of the FPGA board which is shown in Figure X. The FPGA board is connected to an optics board which allows to transmit the IGBT gating signals optically to the inverter. Furthermore, one current measurement board and one board for voltage measurements are connected to the FPGA board. The two-phase three-level inverter just consists of two phase legs.

B.2.1 FPGA board

The FPGA board which is shown in Figure X is used for the real-time computer system for the three-level inverter test bench. As the board uses an Altera Cyclone III FPGA with $40{,}000$ logic elements, it is also possible to directly implement control algorithms on the FPGA which is clocked with $20\,\mathrm{MHz}$. The board also has a very fast 12 bit AD converter. It allows to measure all eight different channels simultaneously with up to 65 megasamples per second. Because of this it is also possible to implement highly oversampled control algorithms and safety routines. The measurement boards can be connected to the FPGA board with RJ45 plugs. In order to deliver good measurement results and in order to have less EMI sensitivity, analog differential signalling is used for the measurements.

B.2.2 Two-leg three-level inverter

As already mentioned, the two-leg three-level inverter uses the same design as the version with three phase legs. Another difference is that in this case the complete DC link capacitance is $500\,\mu\mathrm{F}$ and the two flying capacitors both have a size of $500\,\mu\mathrm{F}$, too. For this inverter also a $12\,\mathrm{V}$ power supply is used for the optical interface for the gating signals and to provide auxiliary voltages for the gate drivers.

B.2.3 Loads

As mentioned in chapter X, experimental results were conducted with a resistive-inductive load and for a UPS application. The loads were simply made of discrete components (resistors, inductors, capacitors and diodes for the nonlinear load in UPS configuration).

List of Figures

List of Tables

Bibliography

[1] V. Kaura and V. Blasko, "Operation of a phase locked loop system under distorted utility conditions," *IEEE Transactions on Industry Applications*, vol. 33, no. 1, pp. 58–63, 1997.

[2] P. Rodriguez, J. Pou, J. Bergas, J. I. Candela, R. P. Burgos, and D. Boroyevich, "Decoupled double synchronous reference frame pll for power converters control," *IEEE Transactions on Power Electronics*, vol. 22, no. 2, pp. 584–592, 2007.

[3] M. Ciobotaru, R. Teodorescu, and F. Blaabjerg, "A new single-phase pll structure based on second order generalized integrator," in *2006 37th IEEE Power Electronics Specialists Conference*, 2006, pp. 1–6.

[4] P. Rodríguez, R. Teodorescu, I. Candela, A. V. Timbus, M. Liserre, and F. Blaabjerg, "New positive-sequence voltage detector for grid synchronization of power converters under faulty grid conditions," in *2006 37th IEEE Power Electronics Specialists Conference*, 2006, pp. 1–7.

[5] A. Luna, J. Rocabert, J. I. Candela, J. R. Hermoso, R. Teodorescu, F. Blaabjerg, and P. Rodríguez, "Grid voltage synchronization for distributed generation systems under grid fault conditions," *IEEE Transactions on Industry Applications*, vol. 51, no. 4, pp. 3414–3425, 2015.

[6] S. Golestan, M. Monfared, F. D. Freijedo, and J. M. Guerrero, "Dynamics assessment of advanced single-phase pll structures," *IEEE Transactions on Industrial Electronics*, vol. 60, no. 6, pp. 2167–2177, 2013.

[7] P. Rodríguez, A. Luna, I. Candela, R. Mujal, R. Teodorescu, and F. Blaabjerg, "Multiresonant frequency-locked loop for grid synchronization of power converters under distorted grid conditions," *IEEE Transactions on Industrial Electronics*, vol. 58, no. 1, pp. 127–138, 2011.

[8] A. Cherubini, A. Papini, R. Vertechy, and M. Fontana, "Airborne wind energy systems: A review of the technologies," *Renewable and Sustainable Energy Reviews*, vol. 51, pp. 1461 – 1476, 2015. [Online]. Available: http://www.sciencedirect.com/science/article/pii/S1364032115007005

[9] T. Geyer, “A comparison of control and modulation schemes for medium-voltage drives: Emerging predictive control concepts versus PWM-based schemes,” *IEEE Transactions on Industry Applications*, vol. 47, no. 3, pp. 1380–1389, May 2011.

[10] N. A. Ameen, A. A. Naassani, and R. Kennel, “Design of a digital system dedicated for electrical drive applications,” *EPE Journal*, vol. 20, no. 4, pp. 37–44, Dec. 2010.